Institute of Meteorology, Climatology and Remote Sensing
Department of Geography – University of Basel

EBEX2000
ENERGY BALANCE
OF AN IRRIGATED COTTON FIELD

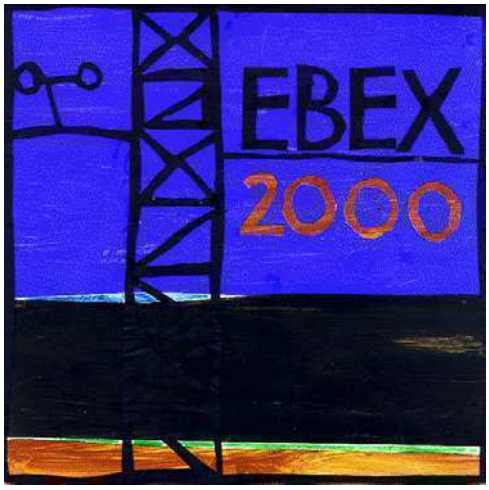

DIPLOMA THESIS

Irene Lehner

Head of the Institute: Prof. Dr. Eberhard Parlow
Supervisor: Dr. Roland Vogt

March 2003

Acknowledgment

I want to express my sincere thanks to all the people who supported me in every imaginable way throughout this work.

I am most grateful to Dr. Roland Vogt, whose verve for micrometeorology and whose perserverence to see into the things and to analyse them is exceptional and contagious.

Special thanks go to Eva van Gorsel, who shared the room with me and therefore was always the first person confronted with my questions as well as with my ups and downs.

I express my gratitude to Prof. Eberhard Parlow and again Dr. Roland Vogt for giving me the opportunity to participate in different field campaigns and work-shops, and to work as a student assistant at the Institute of Meteorology, Climatology and Remote Sensing of the University of Basel.

Thanks to Andreas Christen, Dr. Christian Feigenwinter, Eva van Gorsel and Dr. Roland Vogt for ‘suffering’ from the exceptionally hot weather conditions during the field campaign, for their critical comments, profound discussions and motivating words.

A big thankyou to Günter Bing for the reliable computer network.

Thanks a lot for shared coffee breaks and discussions about questions of true importance to the above mentioned as well as to: Fabienne Aerni, Edith Beising, Thomas Kleiber, Mathias Müller, Josette Pfefferli, Roman Portmann, Kaspar Studer and Rainer Weisshaidinger.

Last but not least I would like to thank my parents who always believe in me.

Contents

List of figures

List of tables

Notation

b_0, b_1, b_2	coefficients	( )
C_O	atmospheric concentration of oxygen	( )
c	speed of sound	(m s^{-1})
c_{min}	heat capacity of minerals	(J m^{-3} K^{-1})
c_{org}	heat capacity of organic matter	(J m^{-3} K^{-1})
c_p	specific heat capacity of air at constant pressure	(J kg^{-1} K^{-1})
c_S	specific heat capacity of soil	(J kg^{-1} K^{-1})
c_V	specific heat capacity of air at constant volume	(J kg^{-1} K^{-1})
c_w	heat capacity of water	(J m^{-3} K^{-1})
d	displacement height	(m)
λE	latent heat flux	(W m^{-2})
F	flux density	(m^{-2} s^{-1})
f	normalised frequency	( )
f	Coriolis parameter	( )
G	soil heat flux	(W m^{-2})
g	acceleration due to gravity	(m s^{-2})
H	sensible heat flux	(W m^{-2})
k_O, k_V	extinction coefficients of oxygen and water vapour	(m^{-1})
k_S	thermal diffusivity of soil	(m^2 s^{-1})
L	Obukhov length	(m)
M	molar mass	(kg mol^{-1})
m_a	molar mass of dry air	(kg mol^{-1})
m_O	molar mass of oxygen	(kg mol^{-1})
m_V	molar mass of water vapour	(kg mol^{-1})
n	frequency	(Hz)
p	pressure	(Pa)
Q_A	horizontal advection of energy	(W m^{-2})
q	specific humidity	(g kg^{-1})
$\Re$	gas constant for dry air	(J mol^{-1} K^{-1})
Ri	Richardson number	( )
R_{ld}	downward long-wave radiation	(W m^{-2})
R_{lu}	upward long-wave radiation	(W m^{-2})
R_n	net radiation	(W m^{-2})
R_{sd}	downward short-wave radiation	(W m^{-2})
R_{su}	upward short-wave radiation	(W m^{-2})
$R_{\theta q}$	correlation coefficient of temperature and moisture fluctuations	( )
ΔS	storage term	(W m^{-2})
$S_{w\alpha}(n)$	co-spectrum of vertical wind velocity w and quantity α at frequency n	
T	temperature	(K)
T_S	surface temperature	(K)

T_S	acoustic virtual temperature	(K)
$T_{w\alpha}(n)$	convolution of frequency-dependent transfer function associated with sensors of vertical wind velocity w and quantity α	
t	time	(s)
u, v, w	longitudinal, lateral, and vertical component of wind vector	(m s^{-1})
u_*	friction velocity	(m s^{-1})
$\overline{u'w'}$	kinematic flux of the u-momentum in the vertical	(m^2 s^{-2})
$\overline{w'q'}$	kinematic vertical moisture flux	(g s^{-1} m^{-2})
$\overline{w'\theta'}$	kinematic vertical heat flux	(K m s^{-1})
V	voltage output of a Krypton KH20	(mV)
x_{min}, x_{org}		
x_w, x_a	content of minerals, organic matter, water and air	( )
x, y, z	Cartesian coordinates	
z	height / depth	(m)
α	albedo	( )
β	Bowen ratio	( )
α, β, γ	rotation angles for planar fit	(°)
	sensitivity factor	(K mV^{-1})
ε	dissipation rate of turbulent kinetic energy	( )
ζ	stability parameter	( )
θ	potential temperature	(K)
λ	latent heat of vaporisation	(J kg^{-1})
λ	wavelength	(m)
ρ	air density	(kg m^{-3})
ρ_a	density of dry air	(kg m^{-3})
ρ_O	density of oxygen	(kg m^{-3})
ρ_V	density of water vapour	(kg m^{-3})
τ	flux of momentum	(kg m^{-1} s^{-2})

1. Introduction

The sun is the main source of energy reaching the earth's surface. According to the first law of thermodynamics energy must be conserved. But where is this energy going to? In other words and from a micrometeorological point of view: How does the partitioning between different energy fluxes look like? Are there other important fluxes than the supposed net radiation, sensible and latent heat, and soil heat flux? A better understanding of how energy is partitioned at the earth's surface is necessary for the improvement of regional weather and global climate models, as well as for assessing soil and plant water use or evaporation. Since the 1980's, improvements in methods and instrumentation have made it possible to determine sensible and latent heat flux individually. Beforehand, it was necessary to determine one of the parts of the energy balance (mostly the latent heat flux) as the residual of the others. However, many micrometeorological surface experiments were unable to demonstrate that the energy balance is closed, which would require that the sum of the sensible and latent heat flux equals all other energy sinks and sources. Later, a residual of 10 to 30 % of the available energy has been observed (WILSON ET AL. 2002). Two main approaches for the evaluation of the vertical fluxes of sensible and latent heat exist: profile methods (aerodynamic approach and Bowen ratio-energy balance method) and – such as for the present study – the eddy covariance method. The ideal experimental system for eddy covariance measures all variables directly, accurately and at the same point, using small sensors with fast response and optimised shape to avoid flow distortion. However, typical eddy covariance set-ups (3D-sonic, fast response sensors for scalars) tend to reduce measured turbulent fluxes. Possible reasons for that are: sensor quality, flow distortion by the sensors, methods of flux determination, heterogeneity of the underlying surface, source area, non-stationarity, and disregarded additional fluxes (e.g. meso-scale fluxes, advection).

The primary objective of EBEX2000 (**E**nergy **B**alance **Ex**periment 2000) is to find out the factors causing the discrepancy between the available energy and the energy used by turbulent fluxes. The idea is to exclude complications arising from terrain

inhomogeneities as much as possible and to concentrate on the measurement techniques. Researchers from the following institutions are involved in the experiment: NCAR (National Centre for Atmospheric Research), KNMI (Koninklijk Nederlands Meteorologisch Instituut), Universities of Basel, Bayreuth, Bragança, Budapest, Hongkong, Padua, Wageningen, and the Technical University of Dresden.

The main focus of the study is to illustrate the influence of several corrections on different energy fluxes and therefore on the residual of the energy balance at the earth's surface. A second topic is the attempt to find possible factors causing the non-closure of the energy balance. Chapter 2 gives a short overview of the theory of energy balance and planetary boundary layer as well as of the concepts of turbulence and the eddy covariance method. The site in southern California, the set-up of the experimental field, and the general meteorological situation is introduced in Chapter 3. Furthermore the applied data handling and theoretical background of the corrections are presented in this section. Chapter 4 contains on the one hand the resulting energy balance terms with a focus on the corrections of the turbulent fluxes and on the other hand considerations of the resulting energy balance and especially its closure. Chapter 5 discusses the results of the corrections, possible reasons for the non-closure of the energy balance and finally, a short summary of this study is given.

2. Theory

2.1 Energy balance

2.1.1 General

The energy balance at the earth's surface is fundamental for the dynamics of the planetary boundary layer. The first law of thermodynamics (conservation of energy) makes it possible to formulate a budget equation for the energy flux at the surface.

Assuming the earth's surface as an infinite, plane, and homogeneous interface, with no mass and no heat capacity, there are, in general, four types of energy fluxes discerned: net radiation R_n, sensible heat flux H, latent heat flux λE, and soil heat flux G

$$R_n = H + \lambda E + G \,. \tag{2.1}$$

However in reality, the earth's surface shows horizontal inhomogeneities, it may be partially transparent to radiation (e.g. water), the surface may be uneven or covered by vegetation. Therefore, it is more appropriate to consider the energy balance of a finite interfacial layer, where energy can be stored or released. The storage term ΔS results from the sensible and the latent heat flux divergence within this air column as well as of the energy stored in the biomass. The biochemical energy storage due to photosynthesis is neglected in this study due to its small amount of $1 - 3$ % of R_n. The layer can be treated as bounded by horizontal planes at the top and at the bottom. Therefore it is still possible to regard only the vertical fluxes:

$$R_n = H + \lambda E + G + \Delta S \,. \tag{2.2}$$

If the surface is not horizontally homogeneous (e.g. regarding roughness elements, moisture, surface temperature) or the fetch is insufficient – where fetch refers to an upwind distance with uniform surface characteristics – then the horizontal advection of energy (Q_A) can become significant and has to be taken in account:

$$R_n = H + \lambda E + G + \Delta S + Q_A \,. \tag{2.3}$$

Measured values of the various components of the energy balance at a specific site depend on many factors, such as the type of surface and its characteristics, geographical

location, season, time of day, and weather. These general remarks as well as the following sections regarding the main terms of the energy balance are described in many textbooks such as AYRA (2001) or OKE (1987).

The sign convention employed in this study is: radiation fluxes are defined as positive values if they are directed towards the surface and all other fluxes are defined as positive values if they are directed away from the surface.

2.1.2 Radiation balance

The radiation balance (R_n) can be split in four components: incoming short-wave (R_{sd}), outgoing short-wave (R_{su}), incoming long-wave (R_{ld}), and outgoing long-wave radiation (R_{lu}):

$$R_n = R_{sd} - R_{su} + R_{ld} - R_{lu} . \tag{2.4}$$

Figure 2.1 shows the mean daily course of the radiation balance and its components during EBEX2000 (in pacific daylight time, PDT). A significant fraction of the incident short-wave radiation is reflected back by the surface, depending on the surface albedo. Most vegetated surfaces have an albedo in the range of 10 – 25 % (OKE 1987). The incident short-wave radiation consists of both direct-beam solar radiation and diffuse radiation (the so called global radiation), and shows a strong diurnal course in the absence of clouds. The radiation balance has its minimum shortly after sunset, when global radiation is no longer available, but the terrestrial emission is still relatively high due to the warmed earth's surface. The maximum net radiation falls together with the maximum global radiation.

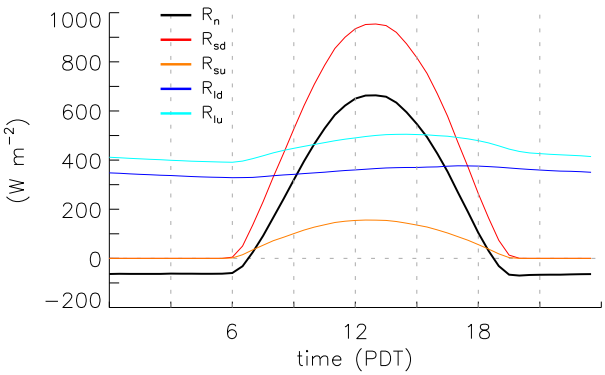

FIGURE 2.1: Mean daily course of the radiation balance and its components (W m^{-2}) during EBEX2000 (DOY 209-239).

2.1.3 Sensible and latent heat flux

Sensible and latent heat flux show a diurnal pattern directly related to solar input. In general, during daytime both fluxes are directed upwards. Their proportion depends mostly on the availability of water for evapotranspiration. A measure for this relationship is the Bowen ratio β. For instance, during EBEX2000 the daytime Bowen ratio is constantly less than one, i.e. latent heat flux exceeds sensible heat flux. This can be explained by the irrigation of the experimental cotton field and therefore the sufficient availability of water for evapotranspiration. At night both fluxes have about the same magnitude but are in opposite direction. Latent heat flux is still upwards, but sensible heat flux is directed towards the surface.

2.1.4 Soil heat flux

The soil heat flux averaged over a whole day is often near zero, but over short time periods the ratio of net radiation going into the soil heat flux may be considerable. An often used estimation is that the soil heat flux is about 10% of net radiation during daytime and up to 50 % at night (OKE 1987). Besides radiation the soil heat flux depends on local atmospheric exchange processes, existing vegetation, soil texture and thermal properties of the subsurface medium. Vegetation reduces direct solar irradiation and increases transpiration and turbulence. If water is available at the soil surface – e.g. after a flood irrigation such as during EBEX2000 – a considerable part of heat is used for evapotranspiration. The thermal properties of the soil – including heat capacity c_S and thermal conductivity k_S – depend on the soil constituents, especially on soil moisture content. The primary transport process in the soil is conduction, which is mainly driven by a temperature gradient. The flow of heat is in the opposite direction to the temperature gradient and with the assumption of a homogeneous soil, it is given by

$$G = -k_S \frac{\partial T}{\partial z}. \tag{2.5}$$

The soil responds to changes of the environmental conditions with a specific time lag, because the temperature gradient must be developed first. The amplitude of the soil heat flux decreases with depth due to the fact that a certain amount of heat is absorbed along the path of propagation (AYRA 2001, HANKS 1992, STULL 1988).

2.2 Planetary boundary layer

The planetary boundary layer (PBL) is defined as the part of the atmosphere which interacts with and reacts to changes at the surface within several hours. Thus, its structure depends strongly on heating and cooling of the earth's surface. The PBL, its structure, characteristics and daily evolution is described in many textbooks (e.g. AYRA 1998, KAIMAL & FINNIGAN 1994, OKE 1987, STULL 1988). The following brief description is based on the above mentioned books.

2.2.1 Characteristics

The state of the atmosphere depends on the following variables: the wind vector $\boldsymbol{U}$ with its longitudinal, lateral and vertical component (u, v, w), temperature T, specific humidity q, pressure p and density ρ. The manner these variables depend on time (t) and space (x, y, z) can be described with the equation of state (ideal gas law) and the conservation equations for mass (continuity equation), momentum, moisture, and heat (first law of thermodynamics). However, the set of equations as a whole is so complex that no analytical solution can be found for boundary layer conditions. Depending on the scale of interest and on the order of magnitude, terms may be neglected or need to be parameterised. The two main simplifications are the assumption of homogeneity and stationarity. Homogeneity is given if the statistical characteristics only vary in the vertical, i.e. they are independent of horizontal position. This assumption is only valid if an adequate fetch is present and therefore the flow can be considered as adapted to the surface. Stationarity is given if the turbulent characteristics do not vary with time. This assumption is never fulfilled in its narrower sense due to synoptic patterns and as essentially all meteorological variables show a diurnal cycle. However, quasi stationary conditions can be achieved by choosing a suitable averaging time, which must generally be long enough to include the significant scales of turbulence.

2.2.2 Structure

Above the PBL is the free atmosphere, where the flow is in near-geostrophic balance and no longer influenced by the surface. The PBL itself is subdivided in a laminar sublayer, the inner layer and the outer layer. In the very thin (only a few millimetres) laminar boundary layer close to the surface, the transport of momentum, sensible and latent heat is by molecular diffusion. The Reynolds number is a measure of the ability of the molecular-viscous forces to absorb the energy of the turbulent movement, or if the flow is getting turbulent. In the inner layer the vertical exchange of momentum, sensible and latent heat is independent on height (varying less than 10 %) and the wind shows a logarithmic profile. The flow is insensitive to the earth's rotation and the wind structure is determined primarily by surface friction and the vertical gradient of temperature. In the outer layer the influence of the surface friction decreases with height, the earth's rotation becomes important and the vertical transport of momentum, heat and moisture is height dependent.

2.2.3 Daily evolution

The daily evolution of the PBL depends strongly on solar input. After sunrise, when the surface is heated the lowest part of the PBL often gets unstable and a convective layer evolves. The resulting turbulence tends to mix heat, moisture, and momentum uniformly in the vertical. Due to the almost negligible turbulence in the free atmosphere, an often sharp temperature increase in the transition zone between the free atmosphere and the convective boundary layer (CBL) develops. The CBL grows throughout the morning and reaches its maximum height of 1 – 2 km in the afternoon. Briefly before sunset, the thermals cease to form and turbulence decays. The remaining, neutrally stratified, residual layer initially maintains the characteristics of the recently decayed CBL. As the night progresses, the earth's surface cools and a stable boundary layer (SBL), which reaches a maximum height of 100 – 200 m, evolves. The statically stable air tends to suppress turbulence. Wind speed just above the surface often becomes light or even calm, while at the top of the SBL a nocturnal low-level jet evolves (see Appendix A).

2.3 Turbulence

Besides radiation, turbulence is the other important process for vertical energy transport in the atmosphere. Turbulence is induced by mechanical or convective mixing. The main characteristic of a turbulent flow is its irregularity. The behaviour of a single air particle in a turbulent flow can be described with the hydro- and thermodynamic basic equations (see section 2.2.1). However, the interactions between the particles are so complex that the velocity field can only be described as a random distribution in time and space, i.e. turbulence can be treated as a stochastic process. Turbulent flows are instationary and consist of many different size eddies. The eddies act as "means of conveyance" for physical characteristics such as momentum, sensible and latent heat. The relative intensity of these different scale eddies define the turbulence spectrum.

The kinetic energy equation identifies mathematical expressions for the physical processes that govern the turbulent kinetic energy of the atmosphere. These processes include the rate at which kinetic energy is converted from the mean flow to the turbulent flow, at which kinetic energy is converted into internal energy, and at which kinetic energy is dissipated. This behaviour is called energy cascade. The equation of turbulent kinetic energy is given by

$$\frac{\partial e}{\partial t} = \underbrace{-\overline{u'w'}\frac{\partial u}{\partial z}}_{\text{I}} + \underbrace{\frac{g}{T}\overline{w'\theta'}}_{\text{II}} - \underbrace{\frac{\partial}{\partial z}\left(\overline{e'w'} + \frac{1}{\rho}\overline{p'w'}\right)}_{\text{III}} - \varepsilon\,, \tag{2.6}$$

where the terms on the right hand side are: (I) shear production: turbulence is rotational and a vortex is aligned by the mean wind shear and stretched. This vortex stretching mechanism is responsible for the energy transfer, (II) buoyant production, (III) turbulent and pressure transport: they represent the transfer of kinetic energy from one level to another but do not contribute to any overall production or destruction of kinetic energy, and the last term is the viscous dissipation. The ratio of shear production and buoyant production leads to well known stability parameters like the Richardson number *Ri* or the Obukhov Length *L*.

2.4 Eddy covariance method

The spectrum of atmospheric motions often shows a gap at time periods of 20 minutes to 1 hour. Therefore, it is possible to isolate the large scale variations from the turbulent ones. This procedure is called Reynolds decomposition. The value of an entity *s* can be split in its mean part $\bar{s}$ and its deviation from the mean s':

$$s = \bar{s} + s'. \tag{2.7}$$

Throughout the remainder of this study an overbar denotes a mean value and a prime a departure from the mean, i.e. a fluctuation.

The mean vertical flux *S* of a given entity *s* is a function of the characteristics of the "transport eddies": density ρ, vertical velocity *w* and volumetric content of the entity of interest *s* (e.g. water vapour). Applying Reynolds decomposition *S* can be written as

$$S = \overline{\left(\bar{\rho} + \rho'\right)\left(\bar{w} + w'\right)\left(\bar{s} + s'\right)}. \tag{2.8}$$

Because the average of the fluctuations is zero and applying the two assumptions of a zero mean vertical velocity $\bar{w}$ and a constant air density ρ, *S* can be written as

$$S = \rho \overline{w's'}. \tag{2.9}$$

In terms of the fluxes of momentum τ, sensible heat *H* and latent heat λE equation (2.9) can be written as

$$\tau = \rho \overline{u'w'} \tag{2.10}$$

$$H = \rho c_p \overline{w'\theta'} \tag{2.11}$$

$$\lambda E = \rho \lambda \overline{w'q'} \tag{2.12}$$

The main advantage of eddy covariance is to translate the signals measured at finite height above the surface into estimates for surface fluxes.

3. MATERIAL AND METHODS

3.1 Site

The experimental site was located 10 km north of Kettleman City (San Joaquin Valley, California, USA). The valley is orientated NW to SE and is bordered in the East by the Sierra Nevada and in the West by the Kettleman Hills. The nearest hills are about 8 km to the South-West (Figure 3.1). The entire area surrounding the site is flat and agricultural. Except the fields North and North-West of the EBEX2000 field, cotton was planted. The cotton was planted in rows that were orientated E-W with a separation of the ridges of about 1 m. These ridges lay about 0.3 m above the interspersed furrows. The cotton canopy was not everywhere closed, but the degree of closure increased during EBEX2000. The canopy height was variable, and is assumed to average 0.9 m. The zero-plane displacement *d* is taken to be 2/3 of canopy height (OKE 1987).

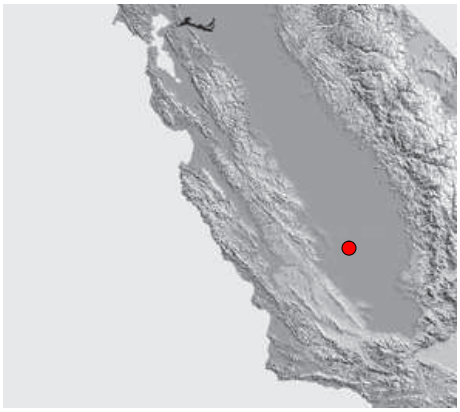

FIGURE 3.1: Relief map of Southern California. The experimental site is indicated by a dot (wwwflag.wr.usgs.gov/USGSFlag/Data/maps/CaliforniaDEM.html).

A special issue is the irrigation of the experimental site. To enable an ideal situation for flood irrigation the cotton field has been mechanically leveled. Hence, the site has a very slight and uniform slope to ESE. The main water channel was in the East of the experimental field (Figure 3.4) and biweekly water was dumped into the furrows. Each day about 100 furrows were flooded. The furrows remained more or less mud for three days and then dried gradually over the remainder of the two weeks. Figure 3.2 shows the irrigation schedule during EBEX2000.

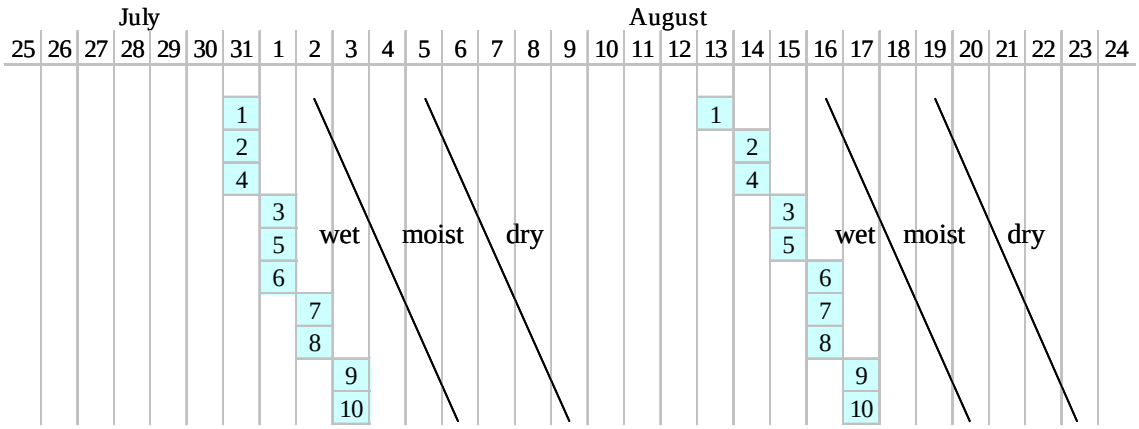

FIGURE 3.2: Irrigation schedule of the date the water arrived at the specified station and the duration of the wet, moist, and dry periods.

3.2 Meteorological conditions

The course of some meteorological parameters from August 01 to August 22 is depicted in figure 3.3. The meteorological situation during EBEX2000 was characterised by high pressure weather. No precipitation was recorded. Due to clear sky conditions the radiation input is high and net radiation reaches a mean daily maximum of 670 W m^{-2}. At night net radiation has a value of about -70 W m^{-2}. The air temperature shows a strong diurnal behaviour with a maximum of typically 30 – 35 °C and a mean daily amplitude of 18 K. The water vapour pressure deficit is high during the whole measurement period. The expected influence of the irrigation in form of an increase of the water vapour content is not obvious, particularly not during the second irrigation period. There is no strong, but a regular diurnal course in wind speed. In general the winds are light with values below 4 m s^{-1} and minima occur in the early morning. Wind direction shows a clear diurnal pattern. In the near-surface layer a nocturnal mountain wind from the Kettleman Hills with directions from 280° to 330° is observed. Shortly after sunrise the mountain wind vanishes and the wind rotates to NW-NE. A special feature is the daily occurrence of a nocturnal low level jet (see appendix A).

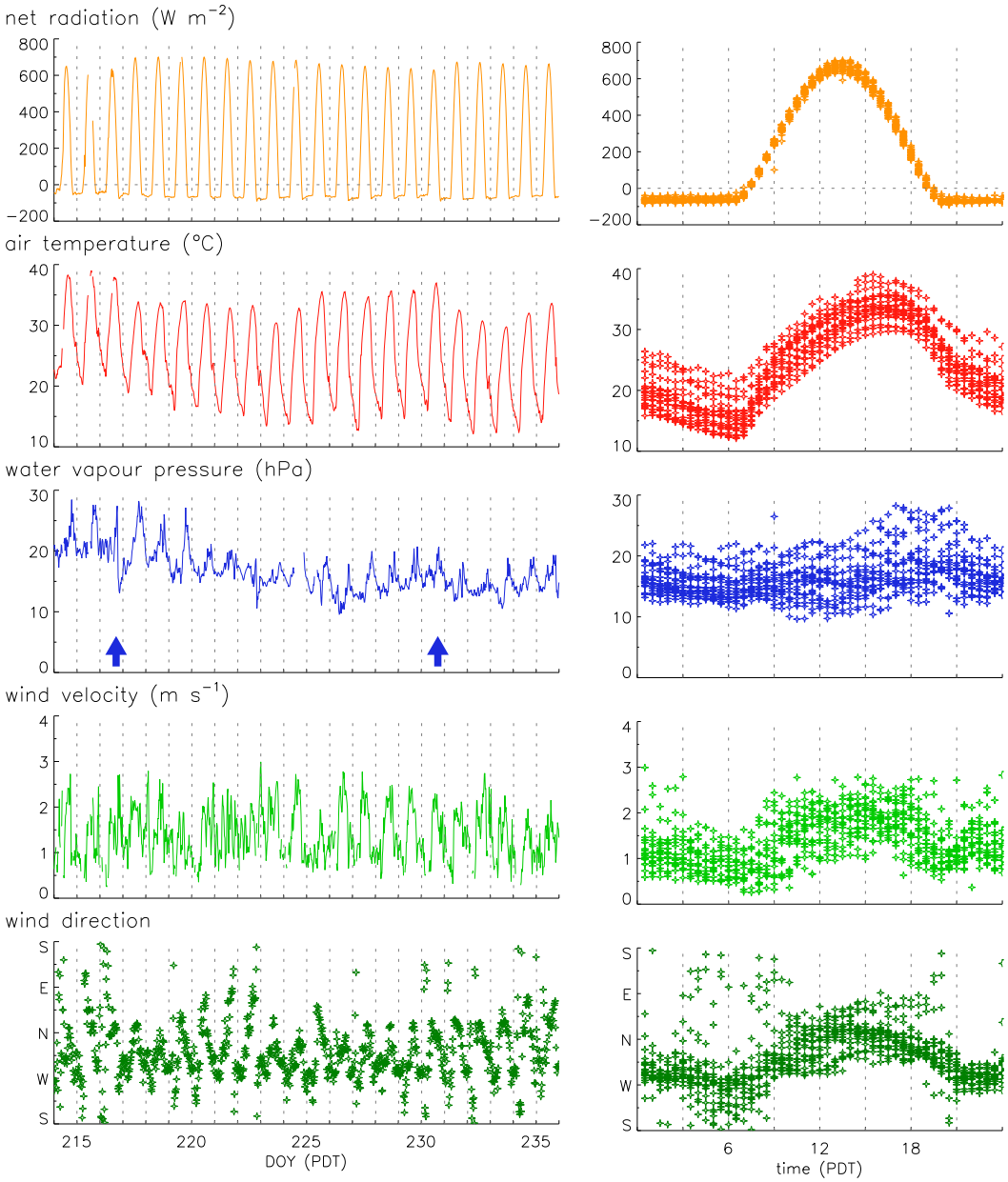

FIGURE 3.3: Course of meteorological parameters from DOY 214 to 235 measured at site 9. Except net radiation the parameters were measured at the profile tower – air temperature and water vapour pressure by a psychrometer and wind velocity by a cup anemometer (Vector Instruments A101L) at a height of 1.5 m, wind direction by a wind vane (Vector Instruments W200P) at a height of 9 m. The arrows in the water vapour pressure graph indicate the arriving water front.

3.3 Set-up and instrumentation

Figure 3.4 shows the set-up of the whole experimental field. At each site – except site 10 – turbulence and radiation was measured. The measurements of the University of Basel were carried out at site 9 (36° 5.8'N, 119° 56'W WGS-84) except the Sodar, which was operated near the trailer. The set-up of site 9 is shown in figure 3.5: three

6 m towers with two levels were set up in a line aligned into the mean wind (320°) and a 9 m profile tower with six levels was operated east of this line. Details of the instrumentation are given in tables 3.1 to 3.3.

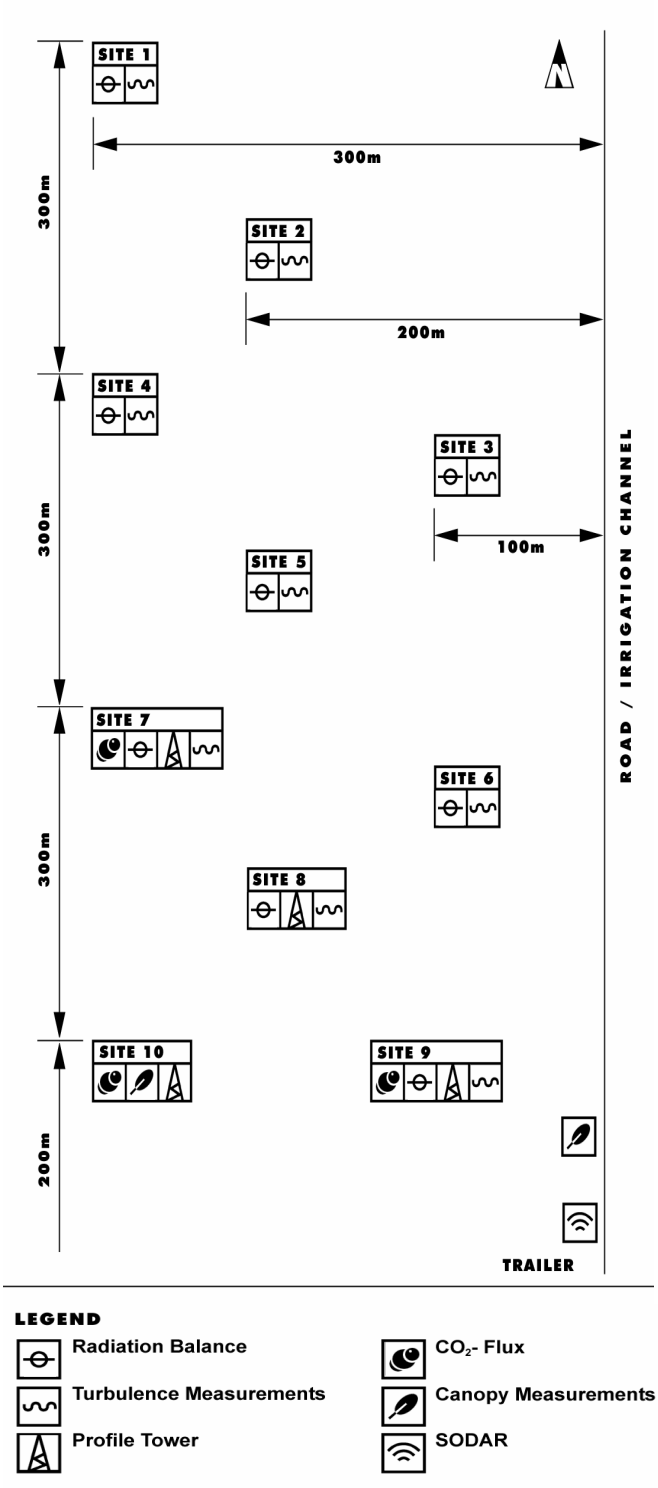

FIGURE 3.4: Schematic of the EBEX2000 field with location of tower sites (adopted from A. Christen).

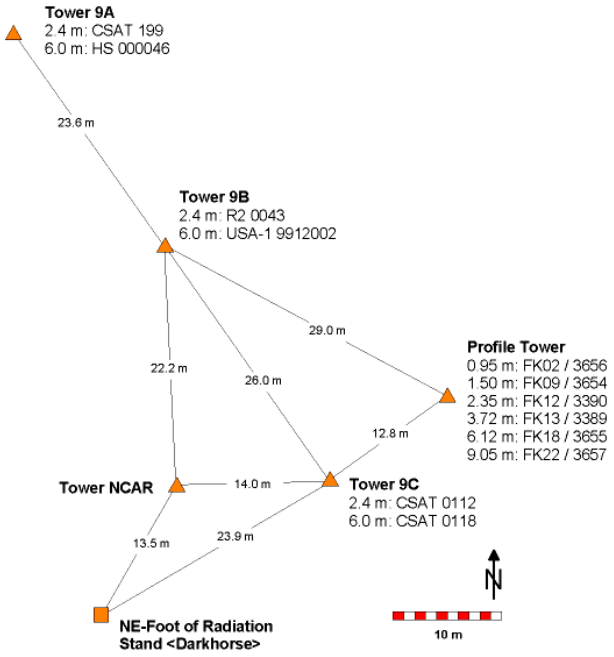

FIGURE 3.5: Set-up at site 9 (adopted from A. Christen).

Including the three sensors from NCAR (R5, R8, R9) the components of radiation balance were measured at site 9 by nine different sensors, which were mounted on a so called 'dark horse' at a height of about 2 m. The dark horse was orientated W-E. Figure 3.6 shows the dark horse and table 3.1 gives some detailed information about the sensors used by the University of Basel.

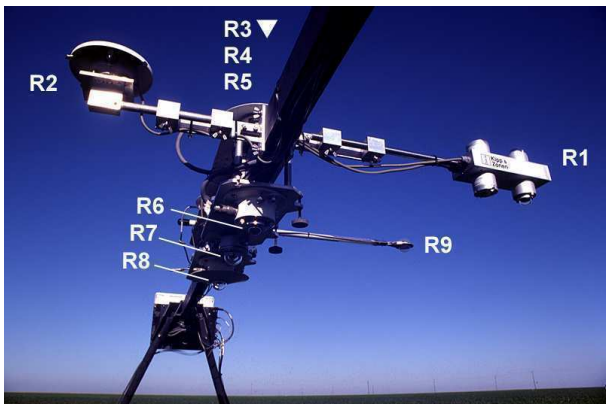

FIGURE 3.6: Instrumentation of the radiation stand at site 9 (looking eastwards).

TABLE 3.1: Radiation measurements by the University of Basel at site 9.

Position	Sensor	Serial No.	Calibration	Measure-ment
R1	Kipp & Zonen CNR1	#980098	manufacturer	R_{sd}, R_{su}, R_{ld}, R_{lu}
R2	Kipp & Zonen CM 21	#910004	manufacturer	R_{sd}
R3	Eppley PIR / WRC	#30323F2	WRC	R_{ld}
R4	Kipp & Zonen CM 21	#950239	WRC	R_{sd}
R6	Eppley PIR / WRC	#31207F3	WRC	R_{lu}
R7	Kipp & Zonen CM 11	#923939	manufacturer	R_{su}

At four places – two within a furrow, two on the slope of a ridge – a heat flux plate and a temperature sensor were buried at a depth of 3 cm. Table 3.2 gives some specifications of the used sensors.

TABLE 3.2: Soil heat flux and soil temperature measurements at site 9.

Position	Sensor	Serial No.	Measure-ment
4th furrow S of dark horse feet	Rimco HFP	#65638	soil heat flux
1st furrow S of dark horse feet	Rimco HFP	#65640	soil heat flux
2nd ridge S of dark horse feet, S-slope	Rimco HFP	#G0057	soil heat flux
3rd ridge S of dark horse feet, N-slope	Rimco HFP	#65628	soil heat flux
4th furrow S of dark horse feet	CS 107	CBT16	soil temperature
1st furrow S of dark horse feet	CS 107	CBT19	soil temperature
2nd ridge S of dark horse feet, S-slope	CS 107	CBT18	soil temperature
3rd ridge S of dark horse feet, N-slope	CS 107	CBT17	soil temperature

At each of the three towers 9A, 9B, and 9C (figure 3.5) two ultrasonic-anemometer-thermometer (short form: sonic) were operated: one at a height of 2.4 m (level 1) and the other at 6 m (level 2). The sonic at position A2 (A2 means tower 9A, level 2 – the same nomenclature is used throughout the remainder of this study) and B1 were both equipped with a Krypton KH20. The system at B2 was run with a LiCor 7500 open path CO_2/H_2O analyser. Details are given in table 3.3.

TABLE 3.3: Sonic measurements at site 9.

Position	Measurement height	Azimuth from N	Sensor	Serial No.	Measurements Calibration	Sampling / Storage	Analog Inputs
A1	2.4 m	323°	CSI CSAT3	#0199	u, v, w, θ wind tunnel matrix 1999	60 Hz/ 20 Hz	-
A2	6.0 m	325°	Gill HS	#000046	u, v, w, θ, q wind tunnel matrix 1999	100 Hz/ 20 Hz	Krypton KH20 #1094
B1	2.4 m	334°	Gill R2	#0043	u, v, w, θ, q wind tunnel matrix 1999	166.6 Hz/ 20.8 Hz	Krypton KH20 #1199
B2	6.0 m	356°	METEK USA-1	#9912002	u, v, w, θ, q, CO_2 wind tunnel matrix 2001	20 Hz/ 20 Hz	LiCor 7500
C1	2.4 m	321°	CSI CSAT3	#0112	u, v, w, θ wind tunnel matrix 1999	60 Hz/ 20 Hz	-
C2	6.0 m	321°	CSI CSAT3	#0118	u, v, w, θ wind tunnel matrix 1999	60 Hz/ 20 Hz	-

3.4 Data processing

3.4.1 Radiation

Data were logged with a sampling rate of 2 s by a Campbell Scientific 23X datalogger. Averages and standard deviations were written into memory every minute. On the basis of the raw data, the values were scaled. Night-time values for short-wave radiation were set to zero. For long-wave radiation measured by an Eppley PIR the method after PHILIPONA ET AL. (1995) was applied (see below). A de-spiking (filter width: two times the standard deviation of 30 minutes) and for missing values a linear interpolation for at most ten minutes was carried out. Afterwards half hourly values were calculated. Each component of the radiation balance was measured at least twice. To get the best composite a sensor comparison was done (see appendix B), which has lead to the use of a sensor combination of the two PIR's, the CM21 #950239 and the CM11.

The method after PHILIPONA ET AL. (1995) was carried out because investigation of the dome temperature revealed important temperature gradients on the dome during measurements. Thus, a single point measurement of the dome temperature is considered to be insufficient. To asses more exactly the representative dome temperature, PHILIPONA ET AL. (1995) suggest to use three thermistors separated by 120° and glued at 45° elevation. Their average generates the used dome temperature. A further

complication arises from the fact that the short-wave and the long-wave part of the radiation spectrum do overlap at their margins and radiation in this range could be counted twice. To avoid this effect sensors have to be shaded from the direct sun. But field tests demonstrate that modified PIR pyrgeometers, i.e. with three dome temperature sensors, can be used unshaded to measure atmospheric and terrestrial radiation with a precision of $\pm$ 2 W m^{-2} (PHILIPONA ET AL. 1995). Thus, for the present data this correction is not carried out.

3.4.2 Soil

Data of the heat flux plates and the soil temperature sensors were sampled, stored and interpolated in a similar manner as radiation data. Since the sensors were buried at a depth of about 3 cm the heat storage in the layer above the sensors was added to the half hourly values derived from the heat flux plates (see below). A sensor comparison has resulted in the assumption that the heat flux plates buried within a furrow were still in contact with air until the second irrigation period (see appendix C). Thus, only the sensors positioned at the slope of a ridge were used to calculate the mean soil heat flux.

Due to change of heat storage in the layer between the soil surface and the sensor, the soil heat flux will be under- or overestimated. To get the soil heat flux at the soil surface G the value of the heat flux plate G_z has to be adjusted. With the simplifying assumptions (i) that the heat flux is in the vertical dimension only, (ii) that there is no other source of heat than insolation, and (iii) that the soil is homogeneous, the additional term depends on the temperature change $\Delta\overline{T_S}$ over time period Δt in the layer Δz between the soil surface and the heat flux plate and the specific soil heat capacity c_S (FUCHS & TANNER 1968):

$$G = G_z + c_S \left(\frac{\Delta \overline{T_S}}{\Delta t} \right) \Delta z \,. \tag{3.1}$$

The average heat capacity of the soil c_S depends on its content of minerals x_{min}, air x_p, water x_w and organic matter x_{org} (VAN WIJK & DE VRIES 1963):

$$c_S = c_{\min}\, x_{\min} + c_{org}\, x_{org} + c_w\, x_w + c_p\, x_p \,. \tag{3.2}$$

The content of organic matter is assumed to be 3 % and the one of minerals 40 %. The content of water was measured and the content of air is the remainder. Typical average values of the heat capacity of the soil components are listed in table 3.4.

TABLE 3.4: Heat capacity for important components of the soil (SCHEFFER & SCHACHTSCHABEL 1998).

	heat capacity (10^6 J m^{-3} K^{-1})
quartz	2.1
clay minerals	2.1
humus	2.5
water	4.2
air	0.0013

3.4.3 Sonic data

For sampling and storage frequency of the sonic data see table 3.3. Raw data were corrected with a sensor specific two dimensional matrix, which was calculated from wind tunnel studies (VOGT 1995). No detrending was carried out. For this study the turbulent fluxes were calculated using the eddy covariance method. For the covariance matrix the coordinate system was additionally rotated into the mean wind applying the planar fit method (see section 3.5.1). The mean, standard deviation and covariance values were calculated on a half hourly basis.

The fluxes of heat and moisture have been corrected for: (i) spectral loss due to sensor line averaging and sensor separation (see section 3.5.2), (ii) the fact that a sonic cannot measure the 'true' but the moisture influenced air temperature and its fluctuations and thus the heat flux will be overestimated (see section 3.5.3), (iii) a non-zero vertical wind velocity due to density fluctuations of moving air parcels (see section 3.5.4) and (iv) the overestimation of the moisture flux due to oxygen absorption by a Krypton KH20 (see section 3.5.5). Density, heat capacity, and latent heat of vapourisation were calculated temperature- and/or moisture-sensitive. Table 3.5 gives an overview of the applied corrections to sonic data. After applying the different corrections gaps, for at most four hours were linearly interpolated.

TABLE 3.5: Overview of the applied corrections to sonic data at site 9.

	A1	A2	B1	B2	C1	C2
spectral loss correction	x	x	x	x	x	x
Schotanus correction	x	x	x	x	x	x
Webb correction	-	x	x	x	-	-
oxygen correction	-	x	x	-	-	-

3.5 Turbulent fluxes

3.5.1 Tilt correction

In practice the coordinate systems of a sonic and the surface will not be perfectly aligned, such that fluctuations in the longitudinal components of the wind appear as vertical velocity fluctuations, and vice versa. Therefore, a tilt correction for these small deviations of the sonic coordinates is needed. There are mainly three methods to determine the orientation of a sonic relative to a Cartesian coordinate system aligned along the mean wind: double rotation, triple rotation and planar fit (for a comparison see appendix D). For the present study the planar fit according to WILCZAK ET AL. (2001) was applied and is briefly described in the following.

The idea is to rotate the original coordinate system such that horizontal velocity components are placed in a plane of the 'real' mean horizontal wind (assuming that it is parallel to the surface) and that the *u*-component is aligned streamline. The orientation of this plane is determined by a least-squares fit of the wind data to the equation:

$$\overline{w}_m = b_0 + b_1 \overline{u}_m + b_2 \overline{v}_m, \tag{3.3}$$

where $\overline{w}_m$, $\overline{u}_m$, and $\overline{v}_m$ are the 30'-averaged measured wind components and the fitted coefficients b_0, b_1 and b_2 are obtained by a multiple linear regression. The tilt angles are calculated for periods delimited by known physical changes in the sonic orientation. Rotation angle α is defined as the pitch angle about the *x*-axis and the roll angle β is measured about the intermediate *x*-axis. These angles are given by the fitted coefficients:

$$\sin\alpha = p_0, \tag{3.4}$$

$$\cos\alpha = \frac{p_2}{\sqrt{{p_1}^2 + {p_2}^2}}, \tag{3.5}$$

$$\sin\beta = \frac{-p_1}{\sqrt{{p_1}^2 + {p_2}^2}}, \tag{3.6}$$

$$\cos\beta = \frac{p_2}{\sqrt{{p_1}^2 + {p_2}^2}}, \tag{3.7}$$

where $p_0 = \frac{-b_1}{\sqrt{{b_1}^2 + {b_2}^2 + 1}}$, $p_1 = \frac{-b_2}{\sqrt{{b_1}^2 + {b_2}^2 + 1}}$, and $p_2 = \frac{1}{\sqrt{{b_1}^2 + {b_2}^2 + 1}}$.

By multiplying data with the matrix given in equation (3.8), they are rotated into a coordinate system that has the *x*-*y*-plane parallel to the ground.

$$P = \begin{bmatrix} \cos\alpha & 0 & \sin\alpha \\ 0 & 1 & 0 \\ -\sin\alpha & 0 & \cos\alpha \end{bmatrix} \begin{bmatrix} 1 & 0 & 0 \\ 0 & \cos\beta & -\sin\beta \\ 0 & \sin\beta & \cos\beta \end{bmatrix}. \tag{3.8}$$

These data can then be rotated into the mean wind direction for each run (i.e. $\bar{v} = 0$) by multiplication by the matrix:

$$M = \begin{bmatrix} \cos\gamma & \sin\gamma & 0 \\ -\sin\gamma & \cos\gamma & 0 \\ 0 & 0 & 1 \end{bmatrix}, \tag{3.9}$$

where γ is the yaw angle about the new *z*-axis and is given by $\gamma = \tan^{-1}\left(\frac{\bar{v}_p}{\bar{u}_p}\right)$.

The planar fit method will lead to non-zero run-mean vertical velocities. The resultant flux contributions reflect the influence of long waves and large eddies on the flux at measurement height.

3.5.2 Spectral loss correction

Measuring and analysing turbulence data leads to spectral loss in the inertial subrange due to physical limitation in sensor size and response, experimental set-up and the data analysis method. This leads to low-pass filtering and thus, the turbulent fluxes will be underestimated. Several approaches exist for the correction of the spectral loss (e.g. MOORE 1986, MASSMAN 2000, HORST 1997).

According to MOORE (1986) the correction ΔF of the flux F of a quantity with specific density α is given by:

$$\frac{\Delta F}{F} = 1 - \frac{\int_0^\infty T_{w\alpha}(n)\, S_{w\alpha}(n)\, dn}{\int_0^\infty S_{w\alpha}(n)\, dn}, \tag{3.10}$$

where $T_{w\alpha}(n)$ is the convolution of frequency-dependent transfer functions associated with sensors of vertical wind velocity w and quantity α. $S_{w\alpha}(n)$ is the atmospheric co-spectrum of w and α at frequency n.

(i) Normalised, parameterised co-spectra

On the basis of the Kansas spectra (KAIMAL ET AL. 1972) the spectra and co-spectra are parameterised by MOORE (1986). Due to the main subject of this paper only the formulae for the co-spectrum of momentum, heat and moisture are mentioned.

For stable conditions ($0 \leq \zeta$) the co-spectra are given by

$$nS_{w\alpha}(n) = \frac{f}{A_{w\alpha} + B_{w\alpha}\, f^{2.1}}, \tag{3.11}$$

where f is the normalised frequency given by $f = \frac{n(z-d)}{u}$ and

$$A_{wT} = 0.284\left(1 + 6.4\frac{z}{L}\right)^{0.75}, \tag{3.12}$$

$$A_{uw} = 0.124\left(1 + 7.9\frac{z}{L}\right)^{0.75}, \tag{3.13}$$

$$B_{w\alpha} = 2.34\, A_{w\alpha}^{\ -1.1}. \tag{3.14}$$

Equation (3.14) follows the publication of MONCRIEFF ET AL. (1997) because of a missing exponent in the paper of MOORE (1986).

For unstable conditions ($-2 < \zeta < 0$) the co-spectra are given by:

$$nS_{uw}(n) = \frac{20.78\, f}{(1 + 31f)^{1.575}}, \qquad f < 0.24 \tag{3.15}$$

$$nS_{uw}(n) = \frac{12.66\, f}{(1 + 9.6f)^{2.4}}, \qquad f \geq 0.24 \tag{3.16}$$

$$nS_{wT}(n) = \frac{12.92\, f}{(1 + 26.7f)^{1.375}}, \quad f < 0.54 \tag{3.17}$$

$$nS_{wT}(n) = \frac{4.378 f}{(1 + 3.8 f)^{2.4}}, \qquad f \geq 0.54. \tag{3.18}$$

For the stable and the unstable case the co-spectra of the vertical moisture flux is assumed to be identical to the co-spectra of the vertical heat flux.

(ii) Spectral transfer functions

Each effect causing a flux loss can be represented by a frequency-dependent transfer function. MOORE (1986) mentions sensor response, sensor line-averaging, lateral and longitudinal sensor separation, and data acquisition (electronic filtering, digital sampling). The time constants of the instruments operated during EBEX2000 are as good as the influence of sensor response can be neglected. Following the publication of HORST (2000) a correction for aliasing associated with digital sampling is not necessary because aliasing affects the individual frequencies but not the spectrum on the whole. RANNIK (2001) mentioned that block averaging has no damping effect on covariance if the block averaging time is much bigger than the filter time constant. Thus, for the existing instrumentation and data acquisition only sensor line-averaging and sensor separation have to be considered. The corresponding transfer functions are described below.

Sensor line-averaging: Theoretically, measurements of a meteorological parameter should be carried out at one point (in a mathematical sense). In practice, the measurement is always done over a finite path (or volume). Thus, turbulent structures like eddies with a smaller diameter than the path length can not be acquired. MOORE (1986) simplified the often used transfer functions for scalar quantities of GURVICH (1962) as:

$$T_p(f) = \frac{1}{2\pi f}\left(3 + e^{-2\pi f} - 4\frac{\left(1 - e^{-2\pi f}\right)}{2\pi f}\right). \tag{3.19}$$

For the vertical wind MOORE (1986) simplified the transfer function of KAIMAL ET AL. (1968):

$$T_w(f) = \frac{2}{\pi f}\left(1 + \frac{e^{-2\pi f}}{2} - 3\frac{\left(1 - e^{-2\pi f}\right)}{4\pi f}\right). \tag{3.20}$$

For both transfer functions the normalised frequency f is calculated by $f = \frac{n\,p}{u}$, where p is the averaging path length.

Sensor separation: If a scalar like water vapour or carbon dioxide is measured, an additional sensor besides the sonic has to be used. To avoid as much as possible a disturbance of the wind field, the two sensors are mounted with a spatial separation. Following Taylor's hypothesis the longitudinal separation is leading to a time shift within the two data series. If the separation is lateral, then the sensors are measuring different parts of the turbulent field. Once again, MOORE (1986) simplifies a more complex approach (IRWIN 1979, KRISTENSEN & JENSEN 1979) and defines the transfer function for both lateral and longitudinal separation as:

$$T_s(f) = e^{-9.9\,f^{1.5}}, \tag{3.21}$$

where the normalised frequency f is calculated by $f = \frac{n\,s}{u}$, where s is the sensor separation.

(iii) Frequency response corrections

With the simplification that the transfer function of the covariance of two variables is equal to the square root of the product of the transfer functions for the variances of the two variables, MOORE (1986) neglects the phase shift inherent in applying a frequency-dependent filter to time-series data (HORST 2000). But this calculation is correct if the time constants of the sensors are equal. Therefore, following MOORE (1986) the total transfer function for momentum, heat, and moisture flux are given by:

$$T_{uw}(n) = T_w(n, p), \tag{3.22}$$

$$T_{wT}(n) = \sqrt{T_w(n, p)\,T_p(n, p)}, \tag{3.23}$$

$$T_{wq}(n) = T_s(n, s)\,\sqrt{T_w(n, p)\,T_p(n, p_q)}. \tag{3.24}$$

3.5.3 Schotanus correction

The operation principle of a sonic is to measure the transit times of ultrasonic signals along a finite path between two transducers. The measurement of the temperature is influenced by humidity and thus, the sensible heat flux is normally overestimated. This problem was first treated by SCHOTANUS ET AL. (1983). The sum of the reciprocals of the transit times are proportional to the sound velocity *c*, which is given by

$$c^2 = \frac{\gamma R}{M} T\left(1+0.51q\right). \tag{3.25}$$

Due to its similarity to the virtual temperature the term $T(1 + 0.51q)$ is called acoustic virtual temperature T_S. This is the temperature measured by a sonic anemometer. From equation (3.25) it follows that T_S equals T only if humidity is zero, which never occurs under field conditions. Thus, to get the real vertical kinematic heat flux $\overline{w'T'}$ the sonic measurement has to be corrected for the influence by humidity. The fluctuations of acoustic virtual temperature correlated with the vertical velocity *w* gives:

$$\overline{w'T'} = \overline{w'T_S'} - 0.51\overline{T}\,\overline{w'q'}, \tag{3.26}$$

which can also be expressed by using an approximate value of the Bowen ratio:

$$\overline{w'T_S'} = \overline{w'T'}\left(1+\frac{0.51\overline{T}\,c_p}{\lambda\beta}\right). \tag{3.27}$$

3.5.4 Webb correction

The simultaneous flux of heat and water vapour causes expansion of the air and thus affects the air density. If the heat flux is upwards, then warmer and less dense air parcels are moving upwards, and colder and denser ones are moving downwards. On the assumption of a zero mean vertical mass flow of air, there must exist a small mean upward velocity. This vertical velocity is very small and not measurable. WEBB ET AL. (1980) expressed it as a function of the turbulent fluxes. They made the following assumptions: (i) the net mean vertical mass flux of dry air is zero, (ii) pressure is constant, (iii) any constituent of air besides dry air and water vapour is negligible, and

(iv) the ideal gas law is valid. The mean vertical velocity is proportional to the water vapour density and its fluctuations:

$$\overline{w} = -\frac{\overline{w'\rho_a'}}{\overline{\rho_a}} = \frac{m_a}{m_v}\frac{\overline{w'\rho_v'}}{\overline{\rho_a}} + \left(1 + \frac{\overline{\rho_v}}{\overline{\rho_a}}\frac{m_a}{m_v}\right)\frac{\overline{w'T'}}{\overline{T}}. \tag{3.28}$$

Taking the vertical flux of water vapour as the mean and the departure from the mean

$$\overline{w\rho_v} = \overline{w}\,\overline{\rho_v} + \overline{w'\rho_v'} \tag{3.29}$$

and using equation (3.28) the corrected flux of water vapour is given by

$$\overline{w'\rho'_v} = \left(1 + \frac{m_a}{m_v}\frac{\overline{\rho_v}}{\overline{\rho_a}}\right)\left(\overline{w'\rho'_{v\,raw}} + \frac{\overline{\rho_v}}{\overline{\rho}}\frac{H}{c_p\,\overline{T}}\right) \tag{3.30}$$

or

$$\overline{w'\rho'_v} = \left(1 + \frac{m_a}{m_v}\frac{\overline{\rho_v}}{\overline{\rho_a}}\right)\left(1 + \frac{\lambda}{c_p}\frac{\overline{\rho_v}}{\overline{\rho}\,\overline{T}}\beta_{raw}\right)\overline{w'\rho'_{v\,raw}}. \tag{3.31}$$

3.5.5 Oxygen Correction

The principle of an open-path hygrometer is to emit ultraviolet light of a specific wavelength at which water vapour absorbs the light. A receiver measures which part of the emitted light is received and the fraction which is absorbed is proportional to the concentration of water vapour. At the used wavelengths of a Krypton KH20 both water vapour and oxygen are absorbed. Therefore, the latent heat flux will be underestimated. TANNER & GREENE (1989) showed that the voltage output V of the hygrometer can be approximated by

$$V = V_0\, e^{-x k_v \rho_v}\; e^{-x k_o \rho_o}. \tag{3.32}$$

Since the signal also includes the fluctuations of oxygen, the density fluctuation has to be corrected. The water vapour fluctuation is given by

$$\rho_V' = \frac{1}{k_V\, x}\left(\ln V - \overline{\ln V}\right) - \frac{k_O}{k_V}\rho_O', \tag{3.33}$$

where the last term on the right hand side of equation (3.33) is the correction due to the hygrometer's response to oxygen fluctuations (TANNER ET AL. 1993). These oxygen

fluctuations are due to pressure and temperature changes and can be evaluated by differentiating the gas law:

$$\rho_O^{'} = \left(\frac{C_O \, m_O}{\Re T} \right) p' - \left(\frac{C_O \, m_O \, p}{\Re T^2} \right) T' . \tag{3.34}$$

Pressure fluctuations are small within common averaging periods and thus the first term on the right hand side of equation (3.34) can be neglected. Taking the covariance of vertical wind speed w and water vapour density ρ_v, gives the vapour flux E

$$E = \frac{\overline{w'(\ln V)'}}{k_V \, x} + \left(\frac{C_O \, m_O \, p}{\Re T^2} \right) \left(\frac{k_O}{k_V} \right) \overline{w'T'} \tag{3.35}$$

The first term on the right hand side is the signal of water vapour and the second term is the oxygen correction depending on the vertical kinematic heat flux. The corrected latent heat flux can be calculated by

$$\lambda E = \lambda E_m + c \, \lambda E_m , \tag{3.36}$$

where the correction factor c is given by

$$c = \frac{C_O \, m_O}{c_p \, m_a} \frac{k_O}{k_V} \frac{\lambda \beta_m}{T} . \tag{3.37}$$

The extinction coefficient for water vapour k_V was determined individually for the used sensors by the manufacturer. For the extinction coefficient for oxygen k_O the value of 0.0045 $m^3 \, g^{-1} \, cm^{-1}$ (TANNER ET AL. 1993) was used.

3.6 Data availability

The measurements were started on July 26 (DOY 208) and were stopped on August 25 2000 (DOY 238). The measurement period for net radiation and soil heat flux is listed in table 3.6. Figure 3.7 shows the data availability for the corrected turbulent fluxes. Due to large gaps in the time series the regarded time period starts only on DOY 218. Before the first cleaning of the Krypton sensors at position A2 and B1 in the late afternoon of DOY 222 the data have an offset and have to be rejected. But for position A2 the covariance of $\overline{w'q'}$ is very well correlated with the data from the LiCor so that

for this instrument the latent heat flux can be calculated anyway. The instruments on position B2 were tore down on DOY 230.

TABLE 3.6: Data availability of net radiation and soil heat flux: start and stop time (PDT) as well as the number of good values.

	net radiation	soil heat flux
DOY of the first value	207.438	207.438
DOY of the last value	238.604	238.584
max. no. half hours values	1448	1447
good values	1430	1429

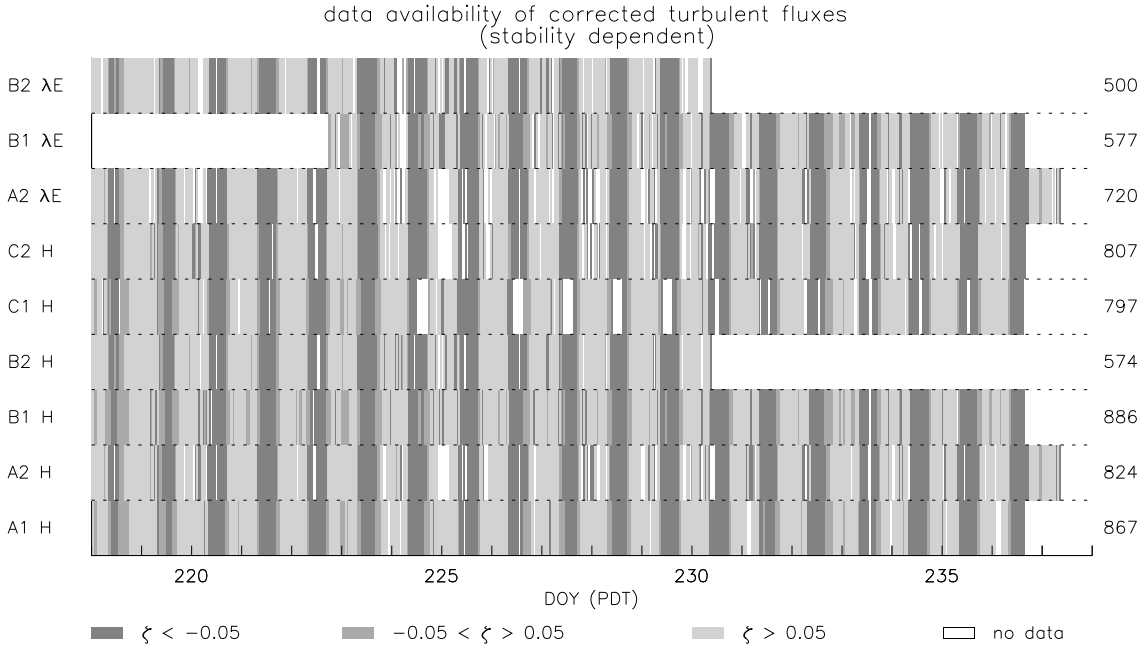

FIGURE 3.7: Data availability of corrected turbulent fluxes (stability dependent). The number on the right indicates the total of “good” half hourly values.

4. RESULTS

4.1 Available Energy

The soil heat flux was calculated as described in section 3.4.2. As the soil surface reacts more rapidly and more intense to solar irradiation, than the soil at a given depth, the applied method after FUCHS & TANNER (1968) leads to a time shift of about an hour and an increase of the magnitude of about 20 % (Figure 4.1). It results in a decrease of the available energy of about 3 % during daytime and an increase of 10 % at night.

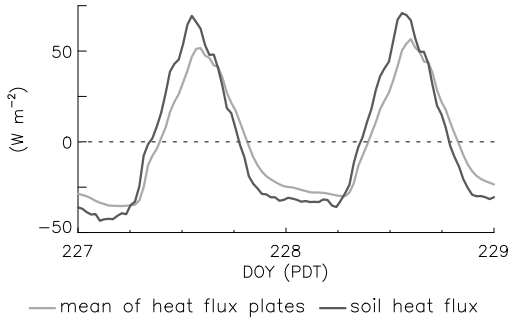

FIGURE 4.1: Course of the soil heat flux and the mean of heat flux plates (W m^{-2}) from DOY 227 to 229.

The course of net radiation R_n, soil heat flux G and the resulting available energy (R_n-G) is depicted in figure 4.2. Net radiation has a daily maximum of 620 – 710 W m^{-2}. Due to clear sky conditions its variation is mainly given by the varying outgoing long-wave radiation – caused by different surface temperatures. This behaviour as well as the great variability of the soil heat flux – up to more than 100 % – is caused by the irrigation of the cotton field. As an average the soil heat flux is about 7 % of net radiation during daytime and 50 % at night. The surface albedo and therefore also the outgoing short-wave radiation, is also influenced by the existence of water on the soil surface but due to the plant coverage only in a small range of 16 – 18 %, i.e. a maximal difference of 20 W m^{-2}. The resulting available energy reaches a mean maximum value of 600 W m^{-2} during daytime and -25 to -50 W m^{-2} at night.

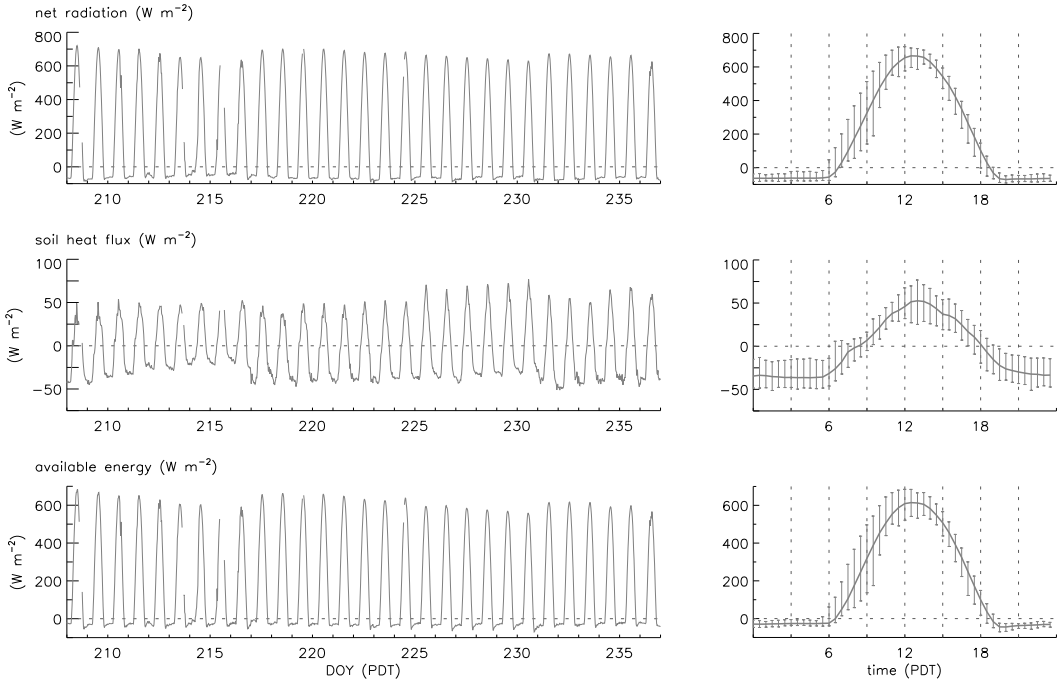

FIGURE 4.2: Course of net radiation, soil heat flux and the available energy from DOY 208 – 236 on the left and mean daily course of the same fluxes of the same time period with indication of minimum and maximum values on the right.

4.2 Turbulent energy

4.2.1 Tilt correction

For the tilt correction the planar fit method, according to WILCZAK ET AL. (2001), was carried out (see section 3.5.1). To get the rotation angles, the whole data set was used for the multiple linear regression. Due to physical changes in the sonic orientation (Figure 4.3) the series of position A2 and C2 had to be split. The rotation angles and the corresponding time periods are listed in table 4.1.

TABLE 4.1: Applied rotation angles for planar fit method.

position	time period (DOY)	α (°)	β (°)	constant ( )
A1	210 – 237	-0.31	1.09	-0.33
A2	210 – 229	-0.37	0.27	0.01
	230 – 237	-0.03	0.83	0.01
B1	210 – 237	2.46	0.90	0.01
B2	210 – 237	-0.20	0.13	-0.08
C1	210 – 237	0.90	-0.01	-0.01
C2	210 – 223	0.13	0.56	0.01
	234 – 237	0.25	0.29	-0.02

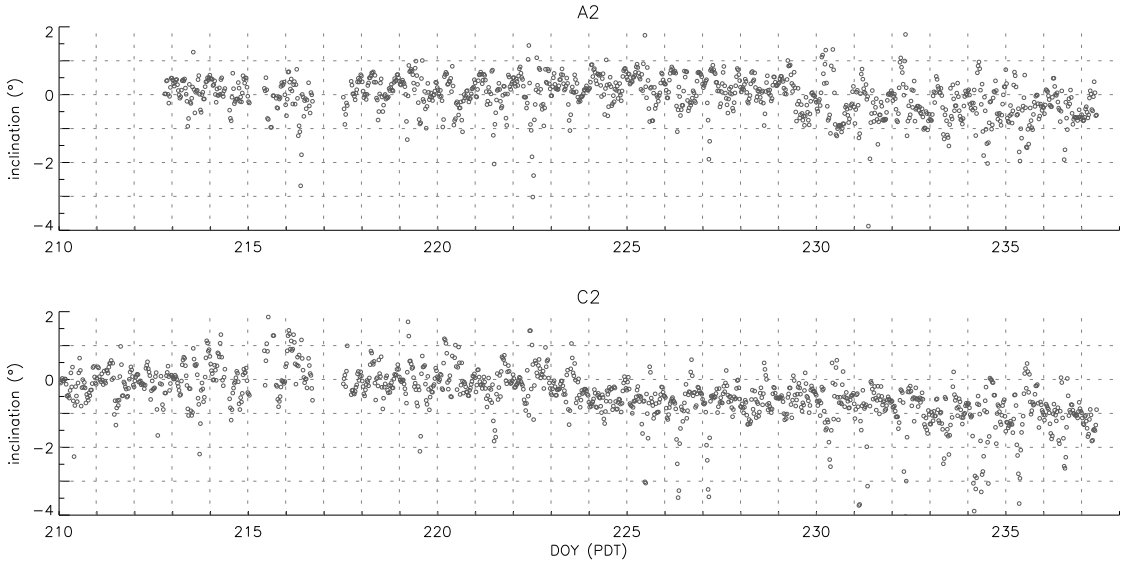

FIGURE 4.3: Course of the inclination from the horizontal plane (°) for position A2 and C2.

To demonstrate the consequence of the application of the planar fit method, figure 4.4 shows wind direction versus mean vertical wind velocity normalized by the mean horizontal wind speed before and after the rotation at position A2. If the sonic is tilted and the local terrain approximates a plane surface, which can be assumed for the EBEX2000 site, then the normalised mean vertical velocity is a sinusoidal function of wind direction (Figure 4.4a). After the planar fit, the normalised vertical velocity should be zero (Figure 4.4b). WILCZAK ET AL. (2001) explain systematic deviation from the sinusoid respectively from zero as flow distortion due to nearby structures.

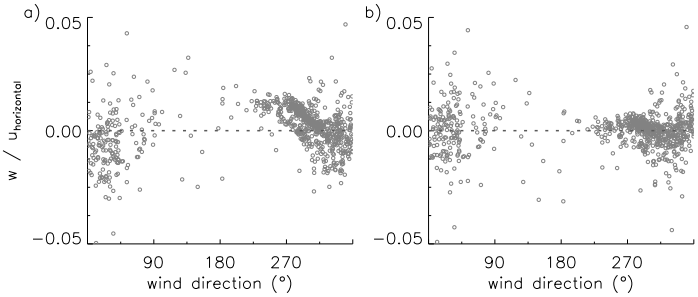

FIGURE 4.4: Wind direction vs. mean vertical wind velocity normalised by the mean horizontal wind speed a) before and b) after applying the planar fit method at position A2.

4.2.2 Spectral loss correction

The turbulent fluxes were corrected for spectral loss due to sensor line averaging and sensor separation according to table 4.2. For details of the correction see section 3.5.2.

TABLE 4.2: Path length and sensor separation (cm) of the sonics at site 9.

	A1	A2	B1	B2	C1	C2
path length (cm)	11.6	15.3	14.7	18	11.6	11.6
sensor separation (cm)	-	25	28	25	-	-

As shown in figure 4.5 the correction term is a function of stability. In the unstable case ($\zeta < 0$) the percentage increase of the turbulent flux is constant. Under stable conditions ($\zeta > 0$) the relative correction is larger and the more stable the atmosphere becomes, the larger the resulting correction is. This behaviour can be explained by the fact that under stable conditions the eddies are smaller and therefore more susceptible to spectral loss.

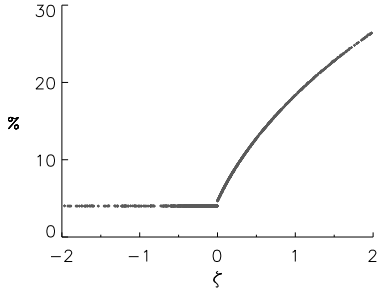

FIGURE 4.5: Dependency of spectral loss correction (%) on stability parameter ζ for latent heat flux during EBEX2000.

The daily course of spectral loss of the sensible and of the latent heat flux is shown in figure 4.6. According to the theory, spectral loss near the ground is larger because the correction is a function of the scale of turbulence and the cospectrum at lower heights shows higher frequencies (KRISTENSEN ET AL. 1997). The magnitude of correction depends furthermore on humidity. The sensible and latent heat flux correction terms exhibit a contrary behaviour. The drier it gets, the larger the correction of sensible heat is, and the smaller the one of latent heat is. For sensible heat flux, only sensor line averaging has to be taken into account and the absolute value of the flux is small,

therefore the correction is small too. At the upper level, the absolute value of the correction remains constant throughout the day (less than 2 W m^{-2}, respectively less than 2 % of the flux). At the lower level, the correction results in marginal higher absolute values (it averages about 2 W m^{-2}, i.e. about 2 % of the flux). In addition to sensor line averaging, sensor separation has to be considered for latent heat flux correction. Although its dependence on irrigation, the latent heat flux constantly shows high values. Hence, the correction results in significant mean values during daytime of 13 W m^{-2} (4 %) at position A2 and B2 and 34 W m^{-2} (14 %) at position B1. At night the mean correction term is less than 3 W m^{-2}.

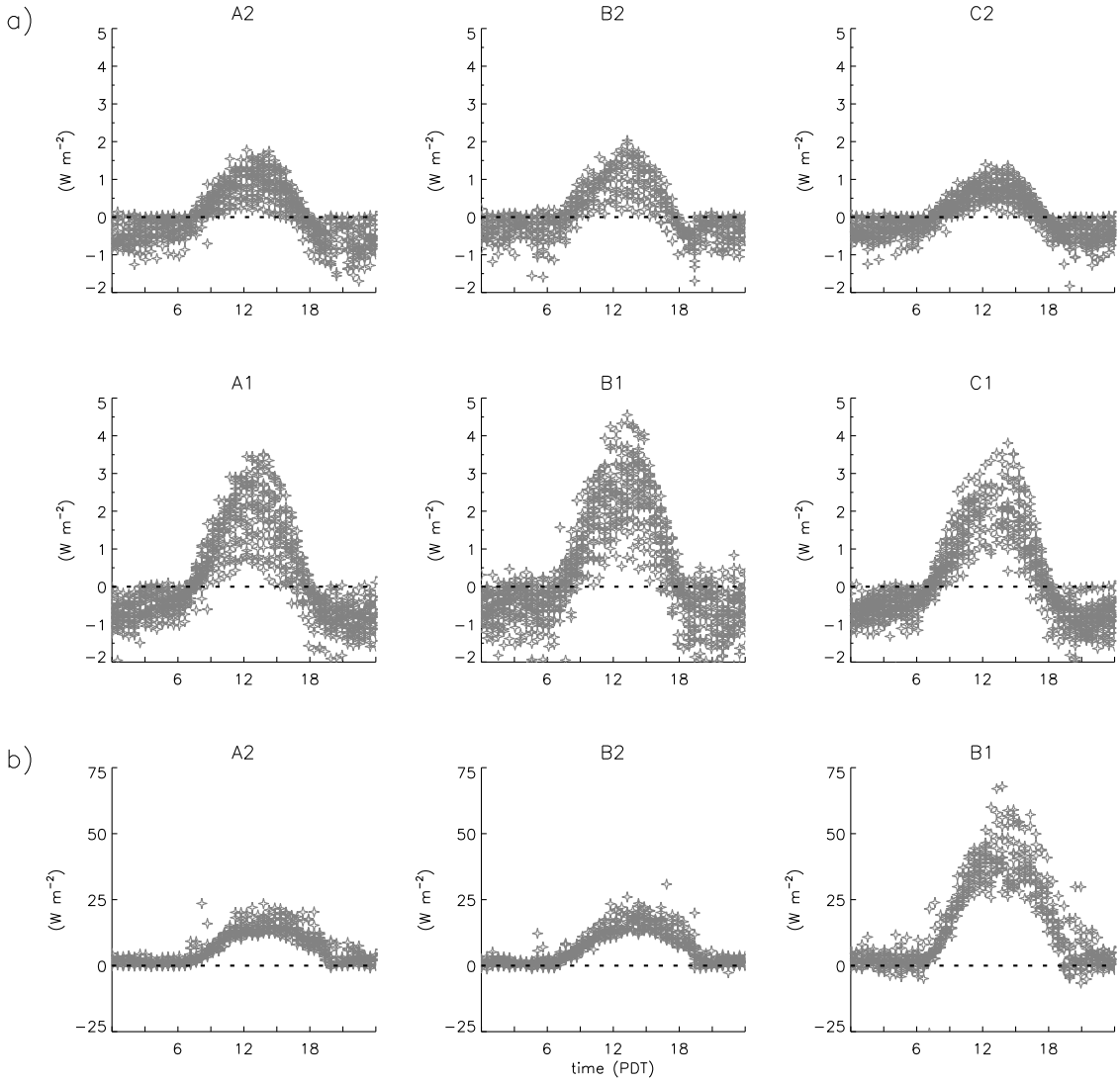

FIGURE 4.6: Daily course of spectral loss (corrected minus uncorrected flux) of a) sensible heat flux, and b) latent heat flux (W m^{-2}).

4.2.3 Schotanus correction

The sensible heat flux, calculated by the eddy covariance method, overestimates the 'true' flux because the temperature measured by a sonic is not the 'true' air temperature but the so called virtual sonic temperature. Hence, the magnitude of the according correction (see section 3.5.3) is particularly a function of humidity. The drier it gets, the smaller the correction term is. Figure 4.7 depicts the daily course of the correction term. The used sensible heat flux for the Schotanus correction is the flux corrected for spectral loss. For the sonics at positions, where humidity was not measured, the values of the humidity sensor at another position were used. At night the sensible heat flux is reduced only by a few watts per meter square (it averages about 1 W m^{-2}). During daytime the correction becomes significant with a mean diminution of about 20%, i.e. 20 W m^{-2} at the lower level and 25 W m^{-2} at the upper level.

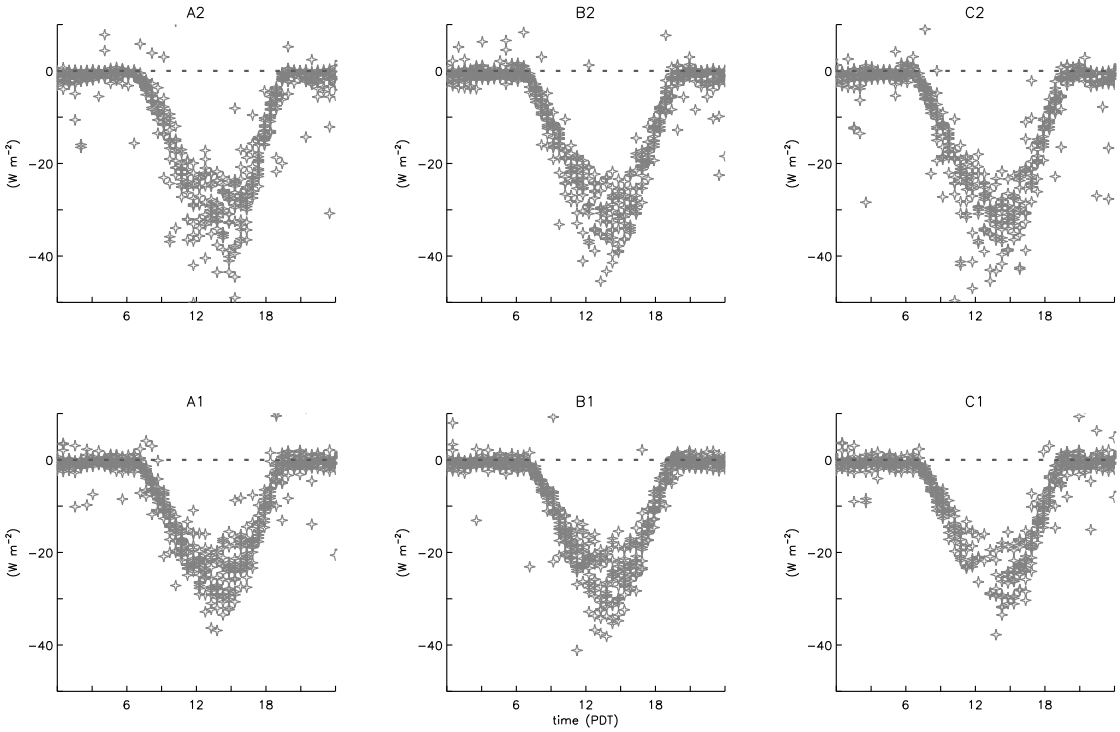

FIGURE 4.7: Daily course of Schotanus correction (corrected minus "uncorrected" flux, W m^{-2}).

4.2.4 Webb correction

The Webb correction (see section 3.5.4) was carried out for the latent heat flux. The correction term is a function of the Bowen ratio β (Figure 4.8) and thus also a function of humidity. In the range $-0.2<\beta<1$ the Webb correction leads to an increase of the latent heat flux. This is the case during daytime. At night and already in the late afternoon sensible heat flux is directed downward and latent heat flux is directed upward. Thus, the Bowen ratio is negative and the correction leads to a slight decrease of the latent heat flux (less than 5 W m^{-2}). The wetter it is, the steeper the regression line between the correction factor and the Bowen ratio is.

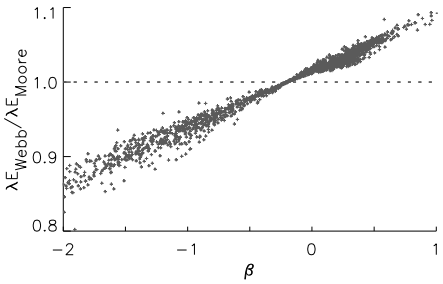

FIGURE 4.8: Webb correction factor as a function of Bowen ratio.

Figure 4.9 shows the daily course of the correction term. During daytime the latent heat flux is augmented by 10 W m^{-2}, i.e. 3.5 %. At night the Webb correction averages a slight diminution of about 1 W m^{-2}. The first days after an irrigation the increase is about 10 W m^{-2}, during dry periods about 15 W m^{-2}. The used latent heat flux for Webb correction is the flux corrected for spectral loss.

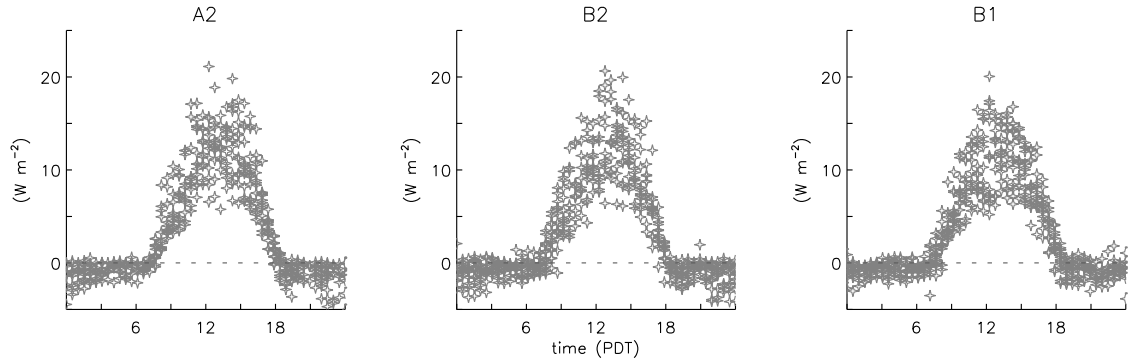

FIGURE 4.9: Daily course of Webb correction (corrected minus "uncorrected" flux, W m^{-2}).

4.2.5 Oxygen correction

At position A2 and B1 the water vapour content and its fluctuations were measured by a Krypton KH20 which has to be corrected for the fact, that within the emitted wave length the light is absorbed by both water vapour and oxygen. Therefore, the latent heat flux is underestimated (see section 3.5.5). The correction term is primarily a function of the Bowen ratio (see eq. 3.37). The smaller the Bowen ratio is, the smaller the resulting correction term is. The daily course of the correction term for the latent heat flux is shown in figure 4.10. During daytime the oxygen correction results in an increase of about 2 %, i.e. 5 W m^{-2}. At night the correction is about 5 % and negative (because of the oppositely oriented fluxes of sensible and latent heat), but due to the small absolute values of the latent heat flux only a few watts per meter square. The used latent heat flux for oxygen correction is corrected for spectral loss and also Webb correction is applied.

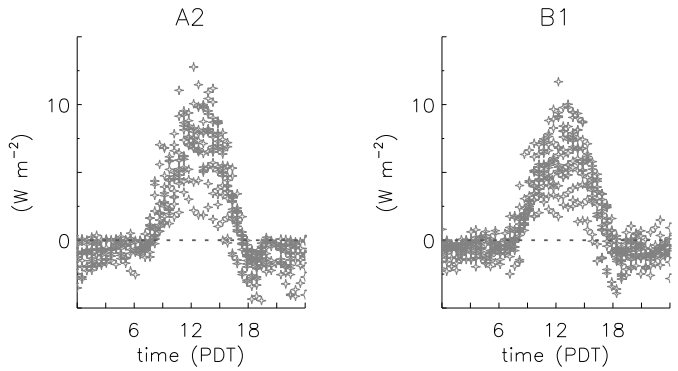

FIGURE 4.10: Daily course of oxygen correction term for latent heat flux (corrected minus "uncorrected" flux, W m^{-2}).

4.2.6 Effect of the corrections and their influence on the energy balance closure

Sensible heat flux: The sensible heat flux is slightly augmented by the application of the spectral loss correction, but considerably reduced by the Schotanus correction. Therefore, the corrections result in a diminution of the sensible heat flux of 12 – 16 % (Figure 4.11). Considering the mean daily course of the correction term, there is only a slight difference in magnitude during daytime between the individual data series. At the lower level the diminution is about 25 W m^{-2}, at the upper about 30 W m^{-2}. At night, the correction remains negligible (less than 5 W m^{-2}).

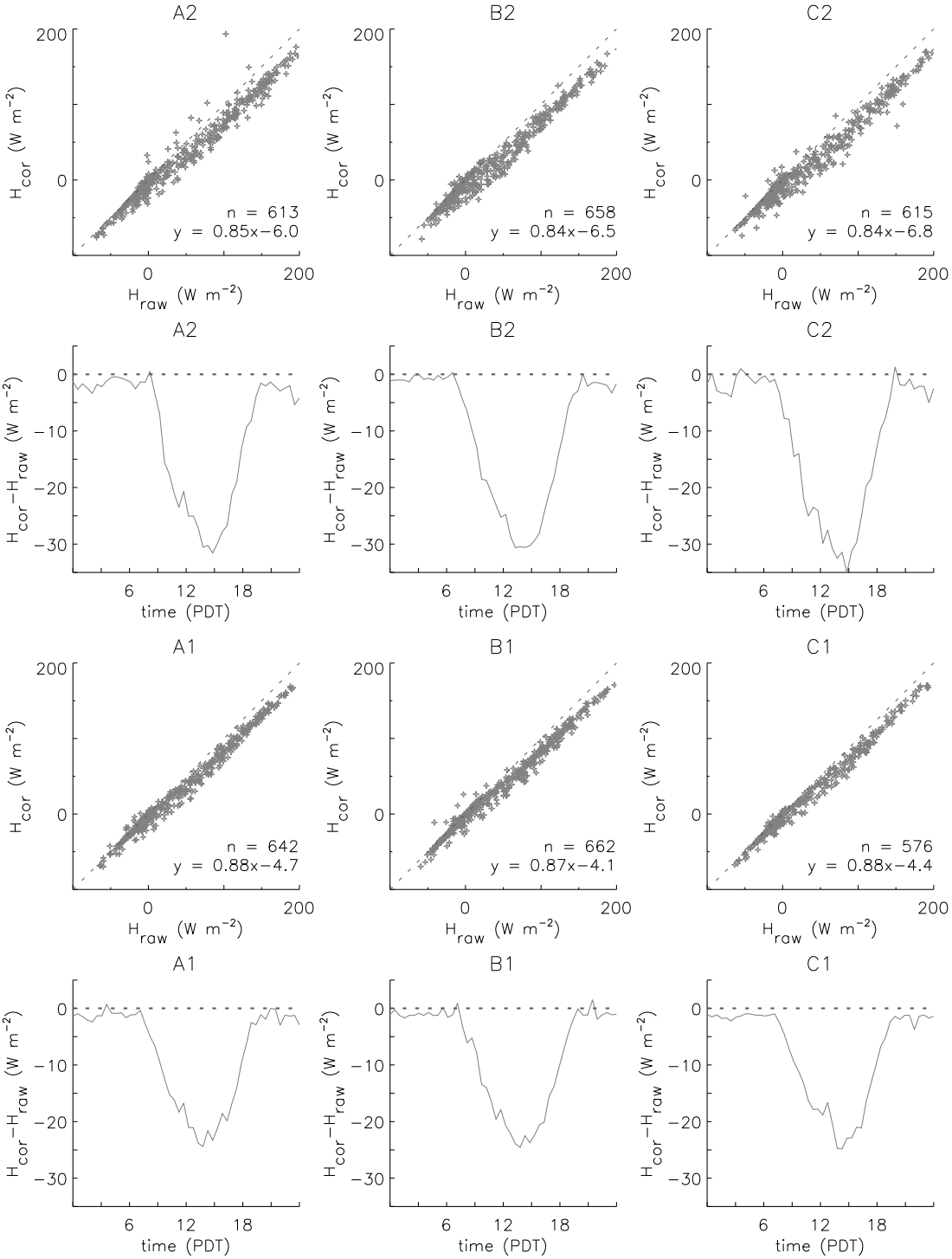

FIGURE 4.11: Raw sensible heat flux vs. the corrected flux in the first and the third row (n is the number of values for the linear regression) and mean daily course of the difference (corrected minus raw flux).

Latent heat flux: All of the corrections applied to the latent heat flux, result in a increase of the flux. Spectral loss correction yields in a rise of about 4 % for the upper level and about 14 % at the lower level. Applying the Webb correction increases latent heat flux by about 3.5 % and deploying the oxygen correction, the flux is augmented by about 2 %. Finally the corrections lead to a rise of the latent heat flux from 7 to 19 % (Figure 4.12). Remember that the oxygen correction is only carried out for the data of position A2 and B1. As displayed in figure 4.12 the mean correction term is insignificant at night. During daytime the two levels differ in magnitude: at the upper level the corrections raise the latent heat flux by 30 – 35 W m^{-2}, at the lower level it is about twice.

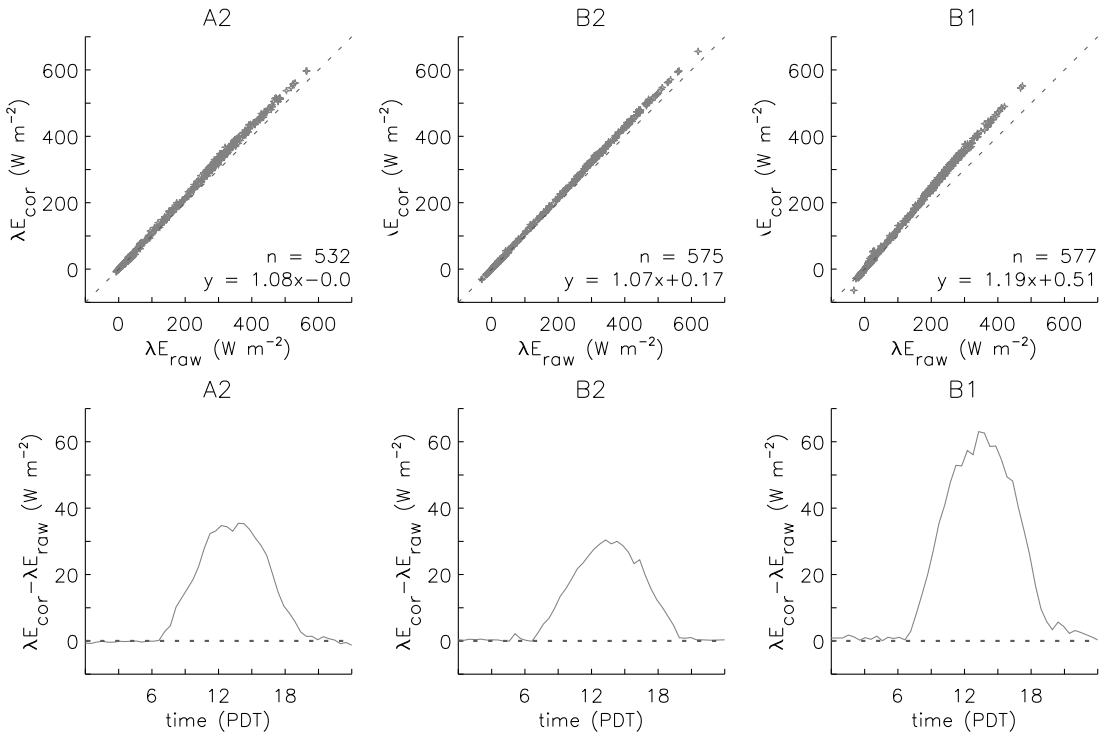

FIGURE 4.12: Raw latent heat flux vs. the corrected flux in the upper row (n is the number of values for the linear regression) and mean daily course of the difference (corrected minus raw flux).

Residual: The applied corrections lead to a change in the residual of the energy balance (Figure 4.13). For the data of the upper level the increase of the latent heat flux is almost compensated by the decrease of the sensible heat flux and therefore the residual is reduced only by 1 – 5 % (less than 10 W m^{-2}). At the lower level the gap of the energy balance can be minimised by 13 % (maximum of 40 W m^{-2}).

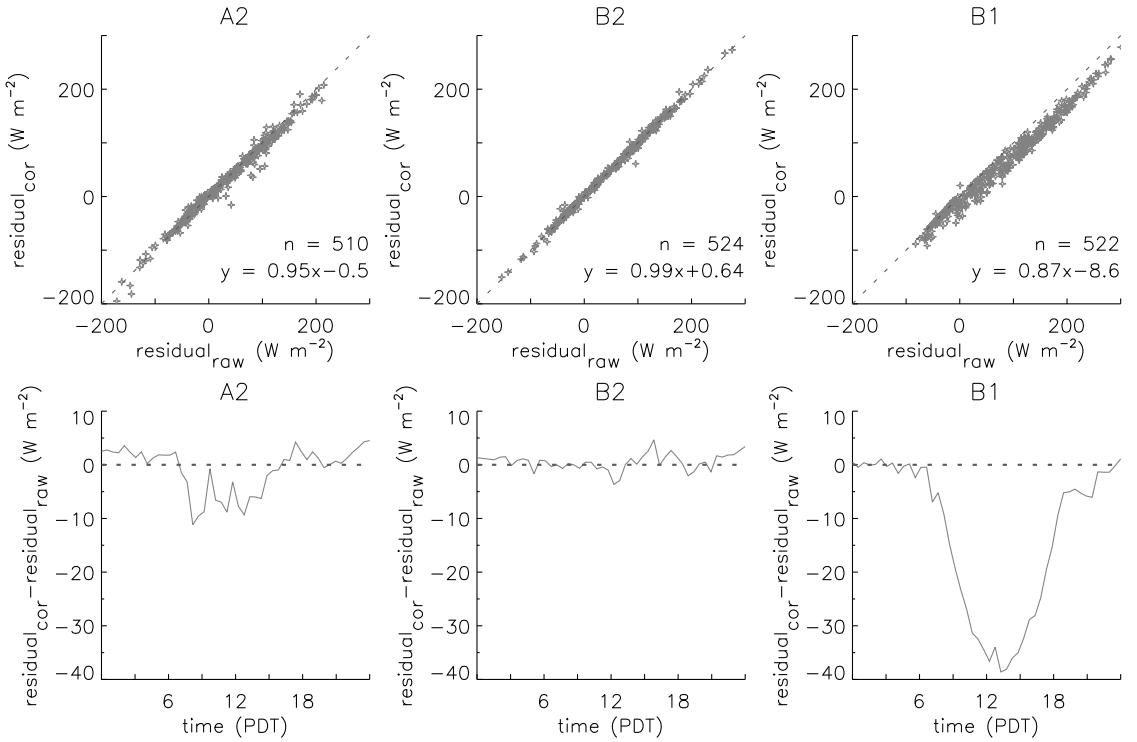

FIGURE 4.13: Residual before vs. the residual after the corrections in the upper row (n is the number of values for the linear regression) and mean daily course of the difference (corrected minus raw fluxes).

4.3 Energy balance

The mean daily course of the energy balance components are diagrammed in figure 4.14, respectively the sensible and the latent heat flux are shown for dry conditions just before (DOY 226 – 228) and wet conditions just after an irrigation (DOY 231 – 233) at position A2.

Net radiation shows only little variation during the whole measurement period. The daily maximum is reached around 1 pm with approximately 660 W m^{-2} and at night the radiative loss is about -70 W m^{-2}. Even the comparison of the wet and the dry situation exhibit no significant differences. During wet conditions the surface temperature is significantly reduced (more than 10 K compared with dry conditions). That results in a smaller loss of long-wave radiation and therefore a slight increase of the radiation balance of about 3 % is given.

Soil heat flux is about 10 % of net radiation during daytime and approximately 50 % at night. It is directed towards the surface from 6 pm to 8 am. Daily maximum and minimum are about ±60 W m^{-2}. The comparison of soil heat flux during dry and wet conditions shows a diminution of the flux after the irrigation of 5 %.

The turbulent fluxes of sensible and latent heat feature a great variability due to the influence of the irrigation. During daytime latent heat flux is twice to fourfold greater than sensible heat flux. Sensible heat flux gets positive in the morning and peaks just after midday (dry conditions: 100 – 150 W m^{-2}, wet conditions: 50 – 100 W m^{-2}). In the late afternoon sensible heat flux changes direction towards the surface and acts as an additional energy source for evapotranspiration, respectively determining a raise of the latent heat flux. This reversal occurs every day, but is more intense and earlier the first days after an irrigation. At night sensible heat flux compensates the also here existing evapotranspiration. The latent heat flux reaches its maximum in the early afternoon, with high values of about 400 W m^{-2} under dry conditions and up to 600 W m^{-2} after an irrigation.

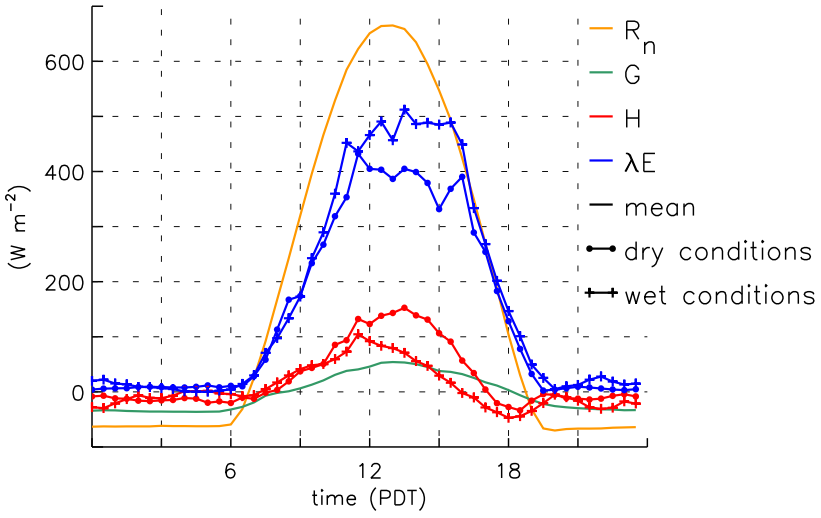

FIGURE 4.14: Mean daily course of energy balance components (W m^{-2}) at position A2.

4.4 Energy balance closure

Energy balance closure, based on half hourly values, is diagrammed in figure 4.15. The closure at position A2, B2 and B1 is 83 %, 77 % and 73 %, respectively. There are a lot of situations, the turbulent fluxes exceed the available energy, particularly for the data of position A2.

Considering the daily course of the energy balance closure (Figure 4.16), it is obvious that closure is poor at night. During daytime closure rises, occasionally up to an over-shooting in the late afternoon. There is not much of a difference in the daily behaviour neither between the two levels nor between dry and wet conditions.

Figure 4.17 depicts the relationship between energy balance closure and wind direction, wind velocity, stability parameter ζ, friction velocity u_* and correlation coefficient of temperature and moisture fluctuations $R_{\theta q}$, respectively, for dry and wet conditions at position A2 and B1 (there is no data for wet conditions a B2). There seems to be a correlation of the energy balance closure with ζ, u_* and $R_{\theta q}$. The closure clearly depends on stability: Under stable conditions closure is poor, under unstable conditions the closure is at least 50 %. The greater the friction velocity is, the better the closure is. When temperature and moisture fluctuations are positively correlated closure is good, when $R_{\theta q}$ is negative closure is poor. These results agree with studies by PRIESTLEY & HILL (1985) or KAIMAL & GAYNOR (1991). A correlation with wind velocity could be expected due to more intense turbulence at higher wind velocities. But, winds are too weak that a dependency is apparent, especially at the upper level. At the lower level a tendency to a better closure with higher wind velocities is recognisable. Wind direction is defined by a well organised daily regime (Figure 3.3) and no obvious correlation with energy balance closure is found. There is not much of a difference between the two levels and the varying conditions concerning the energy balance closure.

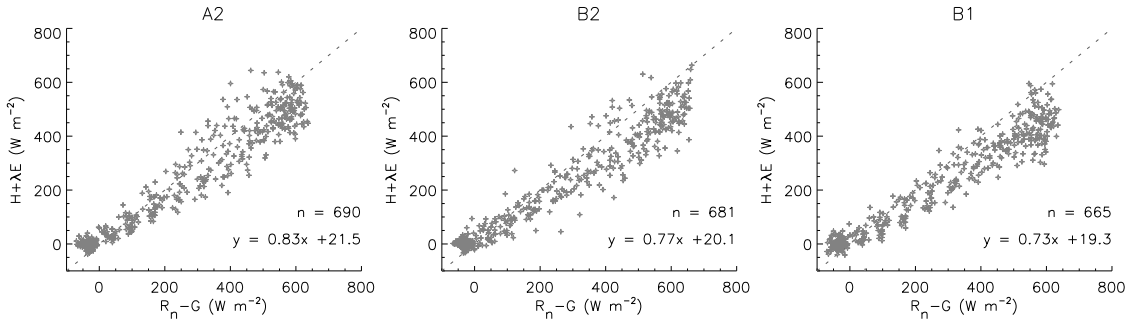

FIGURE 4.15: Comparison of half hourly values of the available energy (R_n-G, W m^{-2}) vs. the turbulent fluxes (H+λE, W m^{-2}) at position A2, B2 and B1.

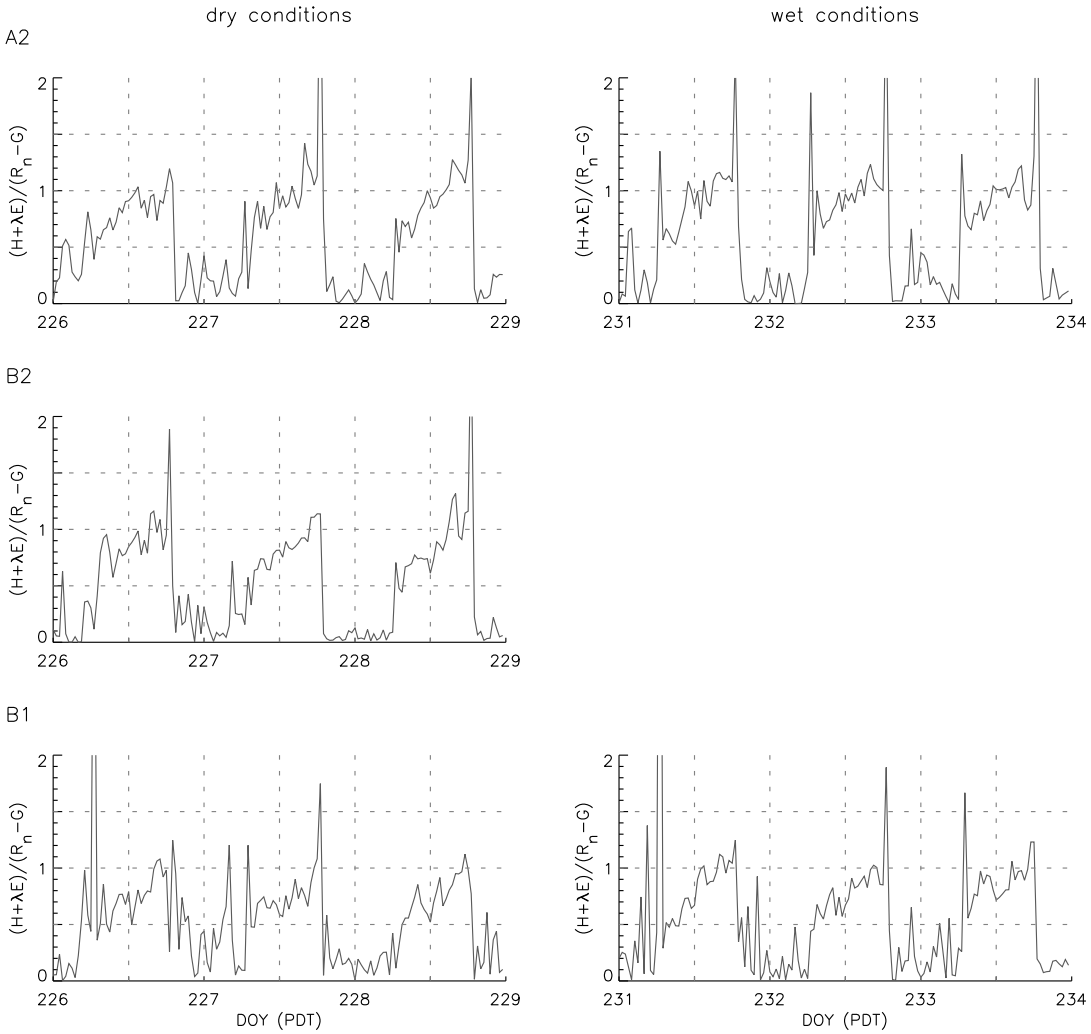

FIGURE 4.16: Comparison of the energy balance closure (H+λE)/(R_n-G) at position A2, B2 and B1 during two time periods, which represent dry (DOY 226 – 228) and wet conditions (DOY 231 – 233).

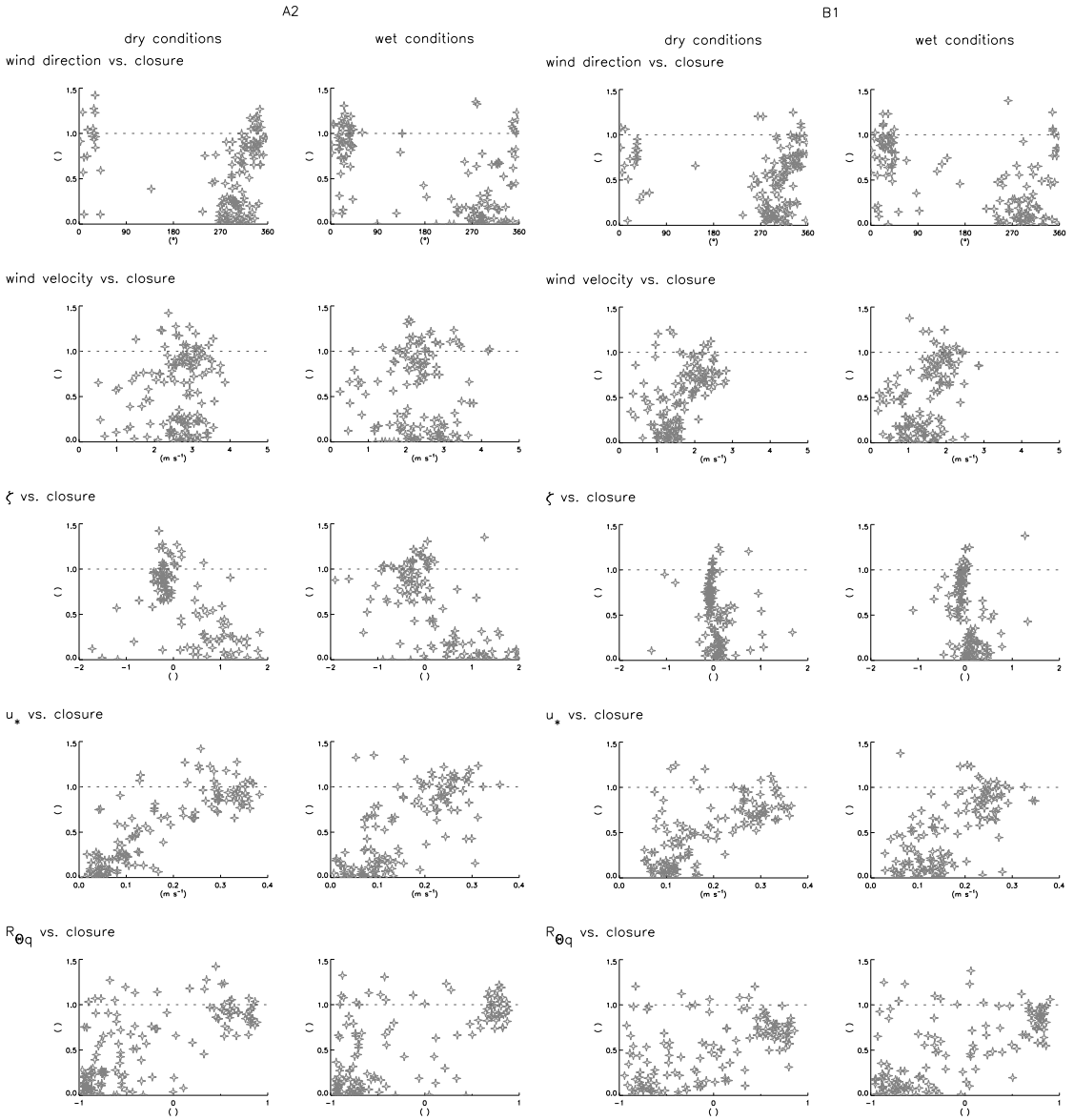

FIGURE 4.17: Closure of the energy balance vs. wind direction, wind velocity, stability ζ, friction velocity u_*, and correlation coefficient of temperature and moisture fluctuations $R_{\theta q}$ during dry (DOY 226 – 228, first and third column) and wet (DOY 231 – 233, second and fourth column) conditions at position A2 (on the left) and B1 (on the right).

The previous energy balance closure considerations are based on half hourly values and particularly, the heat storage term ΔS is not regarded. However, over 24 hours the heat storage term sums to approximately zero and can be neglected. Therefore, the fluxes of the energy balance are added up over 24 hours (Table 4.3). Figure 4.18 shows the course of the daily total of net radiation and soil heat flux, as well as the turbulent fluxes, the Bowen ratio and the residual for position A2, B1 and B2. Despite of fair

weather conditions during EBEX2000, a decrease in net radiation of about 10 % exists. Soil heat flux depends predominantly on soil moisture content and thus, depending on irrigation, the soil acts as a source of energy and under driest conditions as a sink. However, soil heat flux is an almost negligible factor for energy balance closure, because throughout the experiment the amount of the daily total is almost less than 1 MJ m^{-2} day^{-1}, i.e. about 3 % of the energy derived from radiation. Although sensible heat flux was measured at three different positions with three different types of sonics (Table 3.3), the different data series look very similar in behaviour and absolute value. Under wet conditions, the daily total is almost zero or even negative, i.e. regarded over 24 hours the sensible heat flux is directed towards the surface. During dry conditions, sensible heat flux is upwards, but still small compared with latent heat flux (about the fifth part).

TABLE 4.3: Energy balance constituents and residual summed over a full 24 hour cycle (MJ m^{-2} day^{-1}) as well as the ratio $(H+\lambda E)/(R_n-G)$ at position A2, B1 and B2 (a dot indicates no data).

DOY	R_n	G	H			λE			(R_n-G) - $(H+\lambda E)$			$(H+\lambda E)$ / (R_n-G)		
			A2	B1	B2	A2	B1	B2	A2	B1	B2	A2	B1	B2
218	16.63	-0.72	-1.66	-1.22	-1.68	15.70	•	15.02	3.31	•	4.01	0.81	•	0.77
219	16.24	-0.83	-0.69	-0.53	-0.89	14.98	•	15.53	2.78	•	2.43	0.84	•	0.86
220	15.94	-0.63	0.21	0.40	-0.31	15.07	•	15.30	1.30	•	1.60	0.92	•	0.90
221	15.85	-0.82	1.35	1.53	1.40	13.19	•	13.39	2.13	•	1.88	0.87	•	0.89
222	15.62	-0.75	0.82	1.54	0.80	12.09	•	13.25	3.46	•	2.33	0.79	•	0.86
223	14.93	-0.70	2.64	2.22	2.58	11.66	9.86	11.03	1.33	3.55	2.02	0.92	0.77	0.87
224	14.73	-0.86	2.68	2.68	2.35	11.22	10.26	11.31	1.70	2.66	1.93	0.89	0.83	0.88
225	14.85	-0.56	2.13	1.96	2.05	11.55	10.56	11.33	1.74	2.89	2.03	0.89	0.81	0.87
226	14.78	-0.02	1.42	1.82	1.57	12.14	9.93	12.33	1.25	3.05	0.90	0.92	0.79	0.94
227	14.26	-0.32	2.73	2.48	2.17	12.13	9.02	10.87	-0.28	3.08	1.54	1.02	0.79	0.89
228	13.92	-0.16	2.35	2.12	2.02	12.15	9.31	11.28	-0.42	2.64	0.77	1.03	0.81	0.95
229	14.02	0.07	2.87	2.58	2.58	11.22	8.80	11.69	-0.14	2.57	-0.32	1.01	0.82	1.02
230	13.84	0.26	2.53	3.13	•	12.42	9.10	•	-1.37	1.35	•	1.10	0.90	•
231	13.41	0.45	-0.23	-0.16	•	15.12	13.05	•	-1.94	0.06	•	1.15	1.00	•
232	14.13	-0.99	0.14	0.19	•	15.16	12.64	•	-0.18	2.29	•	1.01	0.85	•
233	14.28	-1.17	2.13	1.53	•	12.83	11.91	•	0.49	2.02	•	0.97	0.87	•
234	14.23	-0.97	1.64	1.36	•	11.73	12.34	•	1.83	1.51	•	0.88	0.90	•
235	14.36	-0.43	1.86	1.47	•	11.61	11.20	•	1.32	2.12	•	0.91	0.86	•
236	14.30	-0.35	1.41	•	•	10.64	•	•	2.60	•	•	0.82	•	•
mean DOY 218-236	14.75	-0.50	1.39	1.39	1.22	12.77	10.61	12.69	1.10	2.29	1.76	0.93	0.85	0.89
mean DOY 223-229	14.50	-0.36	2.40	2.27	2.19	11.72	9.68	11.41	0.74	2.92	1.27	0.95	0.80	0.92
mean dry DOY 226-228	14.32	-0.17	2.16	2.14	1.92	12.14	9.42	11.49	0.18	2.93	1.07	0.99	0.80	0.93
mean wet DOY 231-233	13.94	-0.57	0.68	0.52	•	14.37	12.53	•	-0.54	1.45	•	1.04	0.90	•

Latent heat flux shows a similar behaviour for the different data series, with a strong increase just after an irrigation, a steep decrease after a few days and remaining at a lower level under dry conditions. But, there are rather big differences in the degree of the change and the amount of the flux between the two levels. Due to the strong evapotranspiration throughout the experiment, the Bowen ratio is very small: under dry conditions about 0.2 and during wet conditions almost zero. Energy balance closure is much better than based on half hourly values: 98 % at A2, 89 % at B2 and 85 % at B1.

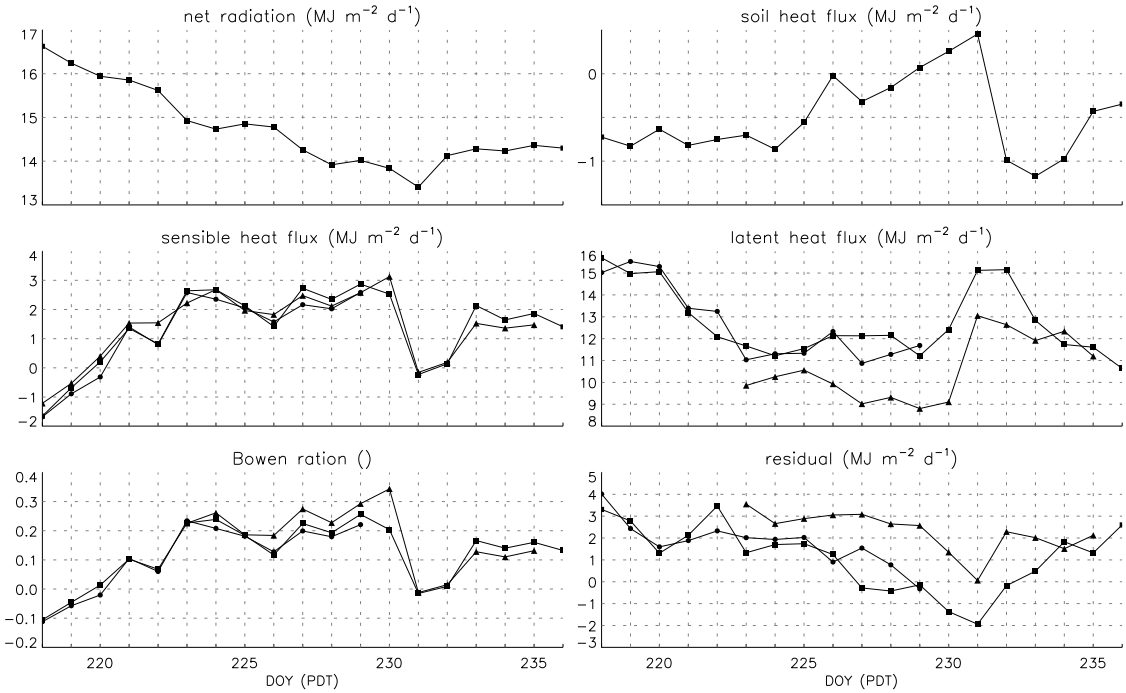

FIGURE 4.18: Course of the daily total of net radiation and soil heat flux, as well as the turbulent fluxes, the Bowen ratio and the residual for position A2 (■), B1(▲) and B2 (●).

5. DISCUSSION

5.1 Corrections

5.1.1 Soil heat flux

The applied method after FUCHS & TANNER (1968) for the energy stored or released within the layer above the sensor, with its resulting time shift and increase of the magnitude of the soil heat flux, is very common and gives reliable results (see sections 3.4.2 and 4.1). However, there are several uncertainties in the use of the method. Under conditions such as during EBEX2000, a little change in the depth of the sensors gives a relative big change in the amount of the correction. And the accurate determination of the depth within a ridge is rather difficult. Another uncertainty is the calculation of the heat capacity because – besides the soil water content – rule of thumb values for the fraction of the soil components were used. But the difference between organic and mineral soil constituents in heat capacity is small and the main factor determining heat dissipation is soil water content. Therefore, the consequence of a false estimation is remote.

5.1.2 Tilt correction

The applied planar fit method (WILCZAK ET AL. 2001) needs many data runs to determine the tilt angles by multiple linear regression (see section 3.5.1). PAW U ET AL. (2000) propose the determination by a surface fit (for example a sinusoidal fit). But a comparison of the linear regression and the sinusoidal fit showed no significant differences in the resulting rotation angles, which is a consequence of the flat terrain. The planar fit method is a statistical method and it is questionable if the number of runs of the present study is sufficient. Particularly, due to the necessary splitting of some data series because of physical changes in the orientation of the sonics, or due to the dominant wind sector from NE to NW or due to the growing vegetation. The resulting rotation angles are quite small. The remaining run-to-run mean vertical velocity is identified by WILCZAK ET AL. (2001) as a result of long waves and large eddies. But what is it exactly? And how does it have to be accounted for in the determination of the

turbulent fluxes? For the present study it is simply ignored. The decision to apply the planar fit anyhow, is due to its lower susceptibility to sampling errors. And a comparison of the planar fit method with the much more common double rotation, shows that the difference between the two methods for sensible and latent heat flux averages about 2 % (see appendix D).

5.1.3 Spectral loss correction

The spectral loss correction according to MOORE (1986, see section 3.5.2) is based on simplifications of the Kansas spectra (KAIMAL ET AL. 1972). These are on the one hand a function of height above zero-plane displacement – the greater the measurement height, the less important are the high-frequency eddies and therefore, the correction is smaller – and on the other hand on atmospheric stability – the more unstable the conditions are, the more the "ideal" cospectra shift to lower frequencies (MONCRIEFF ET AL. 1997). The main restriction for the use of the correction according to MOORE (1986) is, that the spectra should look similar to the Kansas spectra. For the present study this is assumed, but not checked. An other possible source of error are the transfer functions, for which different approaches exist (e.g. MOORE 1986, MASSMAN 2000, HORST 1997, 2000), and the non regarded causes for spectral loss (e.g. data acquisition). High-pass filtering was tried to prevent by choosing a suitable averaging time and the non-application of a linear detrending (RANNIK & VESALA 1999).

5.1.4 Schotanus correction

Due to high humidity values during EBEX2000, the correction after SCHOTANUS ET AL. (1983) results in a significant diminution of sensible heat flux. The correction is widely accepted and applied in many studies (e.g. KAIMAL & GAYNOR 1991, BARR ET AL. 1994, BLANKEN ET AL. 1998, TURNIPSEED ET AL. 2002).

5.1.5 Webb correction

The corrections for the effects of changing air density on gas concentration measurements due to humidity and/or temperature fluctuations according to WEBB ET AL. (1980) results in a mean correction of the latent heat flux of ± 7 %. It is in the same range other studies report (e.g. WILSON ET AL. 2002).

5.1.6 Oxygen correction

The correction of krypton hygrometer data due to the extinction of water vapour by oxygen, needs the extinction coefficients for both water vapour and oxygen. The extinction coefficient for water vapour for the used sensors was individually determined by the manufacturer. For the extinction coefficient for oxygen the value mentioned in TANNER ET AL. (1993) was used. VAN DIJK ET AL. (2003) carried out individual calibrations of several krypton hygrometers for the coefficient of oxygen. Their values show a wide spread, but they are all smaller than the one proposed by TANNER ET AL. (1993). Thus, the resulting correction is smaller too. They conclude, that it is necessary to calibrate the krypton hygrometers individually. Thus, the question arises if the applied correction after TANNER & GREENE (1989) and TANNER ET AL. (1993) overestimates the influence of the extinction of water vapour by oxygen. However, the influence on energy balance would be rather small, because even with the higher value for the extinction coefficient for oxygen the correction is not exceeding 3 % of the latent heat flux.

5.1.7 Conclusions of the applied corrections

As described above, latent heat flux is increased and sensible heat flux is minimised by the applied corrections. At night, they result in a minimal change of the turbulent fluxes of only a few watts per meter square. Thus, the resulting change is within the accuracy of the measurements. Even during daytime the corrections for the data of the upper level cause no significant change of the energy balance (less than 10 W m^{-2}). This is due to the fact that the corrections compensate each other in their effect. Whereas at the lower level the turbulent fluxes are increased by 8 %. The reason for this difference between the two levels, is the effect that the measurements at higher levels are less influenced by

small-scale inhomogeneities of the surface. This means, that it can be assumed that they are really in the constant flux layer, where the assumptions for the eddy covariance method and the corrections itself are mainly given. Additionally, the turbulence spectra is shifted to lower frequencies and therefore, less susceptible for spectral loss. The most part of the difference between the two levels is determined by the spectral loss correction. In comparison with other studies (e.g. MASSMAN 2000, LAUBACH & MCNAUGHTON 1998, TURNIPSEED ET AL. 2002), the resulting corrections for the EBEX2000 data are rather small. This is not astonishing, because most of the corrections depend on sensible heat flux or Bowen ratio. Due to the irrigation both show only small values and in consequence the corrections are small too. However, it seems to be reasonable to apply these corrections, because the deficiencies of the instruments and the necessary set-up are known and – except the spectral loss correction, which is based on statistical similarity – the corrections are based on physical laws. Furthermore if the turbulent fluxes are considered individually, the influence of the corrections becomes significant.

5.2 Energy balance closure

In many studies, where the turbulent fluxes are determined by the eddy covariance method, a residual of the energy balance of 10 – 30 % is reported (WILSON ET AL. 2002, FINNIGAN ET AL. 2003). The reason is an underestimation of the sensible and the latent heat flux or the overestimation of the available energy. Even over flat and homogeneous surfaces and short vegetation, which are presumably ideal conditions for the application of the eddy covariance method, this lack is reported. The assumptions, the eddy covariance method is based on, such as homogeneity, stationarity and zero vertical wind velocity, are often violated. The energy balance closure for EBEX2000 shows a pronounced daily course (see section 4.4). The arising questions are: Where does this behaviour come from? Why is the residual so large during night-time? Where does the over-shooting in the late afternoon origin from? What are the responsible processes? Are there other existing sinks and sources of energy than the regarded ones? Do the sensors measure the fluxes in an accurate way? Is there some random noise in the raw data signals? Are there some conceptual deficiencies in the determination of the fluxes?

5.2.1 Instrumentation

For radiation measurements during EBEX2000 no bias in instrumentation is suspected. The used short-wave radiation sensors match the secondary standard classification for a pyranometer of the WMO (World Meteorological Organisation, Genvea Switzerland) and the long-wave sensors are high-end sensors modified according to the proposal of PHILIPONA ET AL. (1995) (see section 3.4.1 and appendix B). Besides, three of four sensors were calibrated at the WRC (World Radiation Center, Davos Switzerland). Therefore, the radiation measurement is taken to be accurate.

The situation for the measurement of the soil heat flux is different. The measurements of the used soil heat flux plates can be inaccurate, because the thermal conductivity of a heat flux plate and the surrounding soil are potentially unequal. Even though heat flux plates typically have a conductivity similar to soil, but thermal properties vary temporally because of changes in soil water content, including the coupled heat transport (VAN LOON ET AL. 1998). In addition they have to be buried in a given depth to avoid solar irradiation and the measured values have to be corrected (see sections 3.4.2 and 4.1). An additional handicap for the EBEX2000 site is the structure of the cotton field with its furrows and ridges. Therefore, several sensors were buried and the idea was to use their mean value to calculate the "true" soil heat flux. Unfortunately, the "furrow-sensors" are obviously influenced by solar irradiation due to dry cracks which appear. Thus, their data had to be rejected (see appendix C). That is unfortunate because ridges and furrows are different in their appearance. The latter are only bare soil with direct solar irradiation and flooded after an irrigation, the former are vegetated, thus shadowed and never as wet or dry as the furrows. Therefore, it is suggested that the soil heat flux is underestimated in the present study. However, the soil heat flux is only about 10 % of the net radiation during daytime and thus, its underestimation will be within the accuracy of the measurement and does not significantly influence the energy balance closure and regarding the soil heat flux on a daily basis it is almost negligible.

The failures in instrumentation concerning the determination of the turbulent fluxes are corrected in the present study (see section 3.5). The following topics are regarded: flow distortion, tilt error, spectral loss, moisture influenced air temperature, density fluctuations of moving air parcels and oxygen absorption by a Krypton KH20. The corrections are discussed in section 5.1.

5.2.2 Heterogeneity

The intention of EBEX2000 was to measure the energy balance at an ideal site. With respect to the topography and the meteorological conditions, it is certainly fulfilled. Concerning the vegetation, slight doubts are given, because the cotton has grown during the experiment and the foliage got closer. Additionally, there were big differences in the development of the cotton plants within the experimental site. But the main failure are the temporal and spatial extremely variable humidity conditions caused by irrigation (see section 3.1). Besides, there is no information available about the hydrological situation of the surrounding fields.

Every meteorological point measurement represents a spatial average of the surface conditions. The scale of this spatial average, depends on the type of quantities involved in the measurements, mainly measurement height, stability and intensity of cross-wind turbulence (SCHMID 1997). Considering the situation during EBEX2000, a problem arises in the mismatch of the different source areas. With an adequate fetch the problem could be neglected. But, site 9 is located in the SE-edge of the experimental field (Figure 3.4) and particularly with easterly winds – i.e. the source area of the sonic measurements is situated outside the experimental field and represent unknown surface conditions – and during the days the irrigation started, but has not yet reached the site – i.e. the measurements by a sonic represent moist surface conditions, while the source area of the radiation measurement and soil heat flux represent dry conditions – it is doubtful if an adequate fetch is given due to the moisture inhomogeneities.

The effect of these spatial inhomogeneities are on the one hand the development of internal boundary layers. That means, the adjustment of air passing from one type of surface to a new – in the present study, mainly a change from a moist to a dry surface or vice versa – is not immediate throughout the depth of the boundary layer, but it is generated at the surface and diffuses upward. The layer of air whose properties have been affected by the new surface is referred to as an internal boundary layer (AYRA 2001). Thus, under heterogeneous conditions the different source areas represent different surface conditions.

On the other hand horizontal and vertical advection is initialised by the heterogeneity. As described in section 4.3 latent heat flux is upwards throughout the day, and sensible heat flux changes direction already in the late afternoon. In this case, sensible heat flux

acts as an additional source of energy for evapotranspiration and therefore, latent heat flux can become greater than the available energy. This behaviour is a clear indication of an oasis effect. The strong evaporation from the surface results in a cooling of the surface, which causes a downward sensible heat flux (OKE 1987). The downdrafts, upon reaching the warm moist lower part of the boundary layer, are frequently dryer but not warmer than the surrounding warm moist updrafts (MAHRT 1991) and the descending motions are associated with stationary convective cells. Thus, there is advection of moisture, which has to be regarded in the energy balance.

5.2.3 Non-stationarity

Due to mesoscale motions and the diurnal trend of most of the meteorological variables, the assumption of stationarity is hardly ever fulfilled. Thus, the covariance arising from very low frequency fluctuations is missed. This systematic error is due to the failure to capture all of the largest transporting scales and leads to an underestimation of the flux. The systematic error can be reduced by increasing the scale of eddies included in the flux. But, increasing the record length risks including additional mesoscale variability. The ideal choice of averaging time is long enough to reduce the random error, but short enough to avoid capture of non-stationarity associated with mesoscale and synoptic-scale variability (VICKERS & MAHRT 1997).

5.2.4 Night-time situation

During night-time energy balance closure is poor (see section 4.4). Under stable conditions, gradients of water vapour and temperature are often reverse and the fluxes tend to compensate each other (e.g. Figure 4.14). The stable stratification of the near surface atmosphere suppresses turbulence. The exchange of energy – mainly by mechanically induced turbulence and thus, dependent on surface roughness and wind velocity – is diminished and the stability of the atmosphere is strengthened. The different type of energy exchange processes and the other time scale of these processes make it questionable, if the turbulent fluxes can be determined by the eddy covariance method.

5.2.5 Other sinks and sources of energy

As already mentioned in section 4.4 the heat storage term is not regarded in the present study. On the one hand considering this term over 24 hours, it sums to approximately zero and on the other hand it is assumed to be rather small (about ±10 W m^{-2}).

Due to the above mentioned heterogeneity of the moisture situation, advection is assessed to be an important factor, which could explain at least a part of the non-closure of the energy balance. Several approaches to determine this advective flux from a single tower measurement have been published recently (LEE 1998, 1999, FINNIGAN 1999, FINNIGAN ET AL. 2003, PAW U ET AL. 2000).

5.2.6 Daily fluxes

Regarding the energy fluxes on a daily basis, a different pattern for energy balance closure and its constituents (Table 4.3) is shown. The differences between the positions are mainly given by the differences in latent heat flux (Figure 4.18). It is suggested that the difference between the fluxes at the upper level is particularly given by the different kind of used sensors for the determination of the latent heat flux (A2: Krypton KH20, B2: LICOR7500) and that the greater variability at the lower level is due to the more pronounced influence of surface conditions. The mean energy balance closure at position A2 is rather perfect (98 %) and also the closure at B1 and B2 is ameliorated.

5.3 Summary and conclusions

In this study data measured by the University of Basel during EBEX2000 are analysed. The main focus is on several corrections of the turbulent fluxes, which are determined by applying the eddy covariance method on sonic data of two measurement levels (2.4 m and 6 m). An other topic is the consideration of the energy balance and its closure as well as possible factors causing the mismatch of turbulent fluxes ($H + \lambda E$) and available energy ($R_n - G$).

The influence of the corrections on sensible and latent heat flux at night is within the accuracy of the measurements (a few watts per meter square). During daytime sensible heat flux is reduced and latent heat flux is augmented. At the upper level they

compensate each other in their effect. At the lower level the residual of the energy balance could be minimised by 13 %. The given conditions during EBEX2000, with vigorous changes in water availability due to irrigation, are exceptional. Given by the dependency of most of the corrections on Bowen ratio or sensible heat flux – which are both small in the present study – the corrections result in a rather small effect on the fluxes.

Energy balance closure based on half hourly values is 83 % resp. 77 % at the upper level and 73 % at the lower one. Regarding the daily sums closure is much better: 98 % resp. 89 % at the upper level and 85 % at the lower level. Due to fair weather conditions net radiation shows an almost identical behaviour during the experiment. Soil heat flux depends strongly on the soil moisture content and therefore on irrigation. It is about 10 % of net radiation during daytime and about 50 % at night. The turbulent fluxes show also a great variability due to the extremely changing evapotranspiration. Throughout EBEX2000 latent heat flux is greater than the really small sensible heat flux. A special feature at the irrigated site, is the occurrence of the oasis effect, i.e. in the late afternoon sensible heat flux changes direction and is downward until the next morning. A comparison of energy balance closure with different parameters has not shown a clear correlation. Anyhow, a correlation with wind direction and wind velocity is suggested via the resulting source areas. Due to the apparently existing moisture inhomogeneities the question arises if the different source areas of the different sensors represent the same surface conditions. A comparison of the residual of the energy balance and the stability shows two situations: under stable conditions closure is poor, under unstable conditions it is at least 50 %. Greater friction velocity tends to result in a better closure of the energy balance, but during EBEX2000 frictions velocity is too small to shows a clear pattern. The same results from a comparison of energy balance closure with the correlation coefficient of temperature and moisture fluctuations.

Therefore, the applied corrections seem to improve energy balance closure, and none of the regarded parameters could explain the remaining residual. Regarding advective terms seems to be a possibility to ameliorate the situation.

References

AYRA, S.P. (2001): *Introduction to micrometeorology*. Academic Press, San Diego.

BARR, A.G., KING, K.M., GILLESPIE, T.J., DEN HARTOG, G., NEUMANN, H.H. (1994): A comparison of Bowen ratio and eddy correlation sensible and latent heat flux measurements above deciduous forest. *Boundary-Layer Meteorol.*, **71**, 21-41.

BLACKADAR, A.K. (1957): Boundary layer wind maxima and their significance for the growth of nocturnal inversions. Bull. *Am. Meteorol. Soc.*, **38**, 283-290.

BLANKEN, P.D., BLACK, T.A., NEUMANN, H.H., DEN HARTOG, G., YANG, P.C., NESIC, Z., STAEBLER, R., CHEN, W., NOVAK, M.D. (1998): Turbulent flux measurements above and below the overstory of a boreal aspen forest. *Boundary-Layer Meteorol.*, **89**,109-140.

DAVIES, P.A. (2000): Development and mechanisms of the nocturnal jet. *Meteorol. Appl.*, **7**, 239-246.

DWD (1987): *Allgemeine Meteorologie*. Selbstverlag des Deutschen Wetterdienstes, Offenbach am Main.

FINNIGAN, J.J. (1999): A comment on the paper by Lee (1998): "On micrometeorological observations of surface-air exchange over tall vegetation". *Agric. For. Meteorol.*, **97**, 55-64.

FINNIGAN, J.J., CLEMENT, R., MALHI, Y., LEUNING, R., CLEUGH, H.A. (2003): A re-evaluation of long-term flux measurement techniques. Part I: Averaging and coordinate rotation. *Boundary-Layer Meteorol.*, **107**, 1-48.

FUCHS, M. AND TANNER, C.B. (1968): Calibration and field test of soil heat flux plates. *Soil Sci. Soc. Amer. Proc.*, **32**, 326-328.

GURVICH, A.S. (1962): The pulsation spectra of the vertical component of wind velocity and their relations to the micrometeorological conditions. *Izv. Atmos. Oceanic Phys.*, **4**, 101-136.

HANKS, R.J. (1992): *Applied soil physics – soil water and temperature applications*. Springer Verlag, New York.

HORST, T.W. (1997): A simple formula for attenuation of eddy fluxes measured with first-order-response scalar sensors. *Boundary-Layer Meteorol.*, **82**, 219-233.

HORST, T.W. (2000): On frequency response corrections for eddy covariance flux measurements. *Boundary-Layer Meteorol.*, **94**, 517-520.

IRWIN, H.P.A.H. (1979): Cross-spectra turbulence velocities in isotropic turbulence. *Boundary-Layer Meteorol.*, **16**, 237-243.

KAIMAL, J.C. AND FINNIGAN, J.J. (1994): *Atmospheric boundary layer flows – their structure and measurement*. Oxford University Press, New York.

KAIMAL, J.C. AND GAYNOR, J.E. (1991): Another look at sonic thermometry. *Boundary-Layer Meteorol.*, **56**, 401-410.

KAIMAL, J.C., WYNGAARD, J.C., HAUGEN, D.A. (1968): Deriving power spectra from a three-component sonic anemometer. *J. Appl. Meteorol.*, **7**, 827-834.

KAIMAL, J.C., WYNGAARD, J.C., IZUMI, Y., COTÉ, O.R. (1972): Spectral characteristics of surface layer turbulence. *Quart. J. R. Mel. Soc.*, **98**, 563-589.

KRISTENSEN, L. AND JENSEN, N.O. (1979): Lateral coherence in isotropic turbulence and in the natural wind. *Boundary-Layer Meteorol.*, **17**, 353-373.

KRISTENSEN, L., MANN, J., ONCLEY, S.P., WYNGAARD, J.C. (1997): How close is close enough when measuring scalar fluxes with displaced sensors? *J. Atmos. Oceanic Technol.*, **14**(4), 814-821.

LAUBACH, J. AND MCNAUGHTON, K.G. (1998): A spectrum-independent procedure for correcting eddy fluxes measured with separated sensors. *Boundary-Layer Meteorol.*, **89**, 445-467.

LEE, X. (1998): On micrometeorological observations of surface-air exchange over tall vegetation. *Agric. For. Meteorol.*, **91**, 39-49.

LEE, X. (1999): Reply to comment by Finnigan on "On micrometeorological observations of surface-air exchange over tall vegetation". *Agric. For. Meteorol.*, **97**, 65-67.

MAHRT, L. (1981): The early evening boundary layer transition. *Quart. J. R. Met. Soc.*, **107**, 329-343.

MAHRT, L. (1991): Boundary-layer moisture regimes. *Quart. J. R. Met. Soc.*, **117**, 151-176.

MASSMAN, W.J. (2000): A simple method for estimation frequency response corrections for eddy covariance systems. *Agric. For. Meteorol.*, **104**, 185-198.

MASSMAN, W.J. AND LEE, X. (2002): Eddy covariance flux corrections and uncertainties in long term studies of carbon and energy exchanges. *Agric. For. Meteorol.*, **113**, 121-144.

MONCRIEFF, J.B., MASSHEDER, J.M., DE BRUIN, H., ELBERS, J., FRIBORG, T., HEUSINKVELD, B., KABAT, P., SCOTT, S., SOEGAARD, H., VERHOEF, A. (1997): A system to measure surface fluxes of momentum, sensible heat, water vapour and carbon dioxide. *J. Hydrol.*, **188-189**, 589-611.

MOORE, C.J. (1986): Frequency response corrections for eddy correlation systems. *Boundary-Layer Meteorol.*, **37**, 17-35.

NIEUWSTADT, F.T.M. (1984): The turbulent structure of the stable, nocturnal boundary layer. *J. Atmos. Sci.*, **41**(14), 2202-2216.

OKE, T.R. (1987): *Boundary layer climates*. Routledge, London.

PAW U, K.T., BALDOCCHI, D.D., MEYERS, T.P., WILSON, K.B. (2000): Correction of eddy-covariance measurements incorporating both advective effects and density fluxes. *Boundary-Layer Meteorol.*, **97**, 487-511.

PHILIPONA, R., FRÖHLICH, C., BETZ, CH. (1995): Characterization of pyrgeometers and the accurance of atmospheric long-wave radiation measurements. *Appl. Opt.*, **34**(9), 1598-1605.

PRIESTLEY, J.T. AND HILL, R.J. (1985): Measuring high-frequency humidity, temperature and radio refractive index in the surface layer. *J. Atmos. Oceanic Technol.*, **2**, 233-251.

RANNIK, Ü. (2001): A comment on the paper by W.J. Massman „A simple method for estimationg frequency response corrections for eddy covariance systems. *Agric. For. Meteorol.*, **107**, 241-245.

RANNIK, Ü. AND VESALA, T. (1999): Autoregressive filtering versus linear detrending in estimation of fluxes by the eddy covariance method. *Boundary-Layer Meteorol.*, **91**, 259-280.

SCHEFFER, F. AND SCHACHTSCHABEL, P. (1998): *Lehrbuch der Bodenkunde*. Enke Verlag, Stuttgart.

SCHMID, H.P. (1997): Experimental design for flux measurements: matching scales of observations and fluxes. *Agric. For. Meteorol.*, **87**, 179-200.

SCHOTANUS, P., NIEUWSTADT, F.T.M., DE BRUIN, H.A.R. (1983): Temperature measurement with a sonic anemometer and its application to heat and moisture fluxes. *Boundary-Layer Meteorol.*, **26**, 81-93.

STULL, R.B. (1988): *An introduction to boundary layer meteorology*. Kluwer Academic Publishers Group, Dordrecht.

TANNER, B.D. AND GREENE, J.P. (1989): Measurement of sensible heat and water vapor fluxes using eddy correlation methods – Final report. Prepared for U.S. Army Dugway, Utah.

TANNER, B.D., SWIATEK, E., GREENE, J.P. (1993): Density fluctuations and use of the krypton hygrometer in surface flux measurements. *Management of Irrigation and Drainage Systems, Park City, Utah.*

THORPE, A.J. AND GUYMER, T.H. (1977): The nocturnal jet. *Quart. J. R. Met. Soc.*, **103**, 633-653.

TURNIPSEED, A.A., BLANKEN, P.D., ANDERSON, D.E., MONSON, R.K. (2002): Energy budget above a high-elevation subalpine forest in complex topography. *Agric. For. Meteorol.*, **110**, 177-201.

VAN DIJK, A., KOHSIEK, W., DE BRUIN, H.A.R. (2003): Oxygen sensitivity of krypton and Lyman-alpha hygrometers. *J. Atmos. Oceanic Technol.*, **20**(1), 143-151.

VAN LOON, W.K.P., BASTINGS, H.M.H., MOORS, E.J. (1998): Calibration of soil heat flux sensors. *Agric. For. Meteorol.*, **92**, 1-8.

VAN WIJK, W.R. AND DE VRIES, D.A. (1963): Periodic temperature variations in a homogeneous soil. In: VAN WIJK, W.R.: *Physics of plant environment*. North-Holland Publishing Co., Amsterdam.

VICKERS, D. AND MAHRT, L. (1997): Quality control and flux sampling problems for tower and aircraft data. *J. Atmos. Oceanic Technol.*, **14**, 512-526.

VOGT, R. (1995): Theorie, Technik und Analyse der experimentellen Flussbestimmung am Beispiel des Hartheimer Kiefernwaldes – Ein Beitrag zu den Energiebilanzuntersuchungen im REKLIP. *Diss. Phil.-Nat.-Fak. Univ. Basel.*

WEBB, E.K., PEARMAN, G.I., LEUNING, R. (1980): correction of flux measurements for density effects due to heat and water vapour transfer. *Quart. J. R. Met. Soc.*, **106**, 85-100.

WILCZAK, J.M., ONCLEY, S.P., STAGE, S.A. (2001): Sonic anemometer tilt correction algorithms. *Boundary-Layer Meteorol.*, **99**, 127-150.

WILSON, K., GOLDSTEIN, A., FALGE, E., AUBINET, M., BALDOCCHI, D.D., BERBIGIER, P., BERNHOFER, C., CEULEMANS, R., DOLMAN, H., FIELD, C., GRELLE, A., IBROM, A., LAW, B.E., KOWALSKI, A., MEYERS, T.P., MONCRIEFF, J., MONSON, R., OECHEL, W., TENHUNEN, J., VALENTINI, R., VERMA, S. (2002): Energy balance closure at FLUXNET sites. *Agric. For. Meteorol.*, **113**, 223-243.

Appendix A: Nocturnal low-level jet

A special feature is the daily occurrence of a nocturnal low level jet, which can be seen from Sodar data. THORPE & GUYMER (1977) use a simple slab model to explain it's development. The atmosphere is split in three layers in the vertical (Figure A1): the free atmosphere, and two sub-layers constituting the PBL.

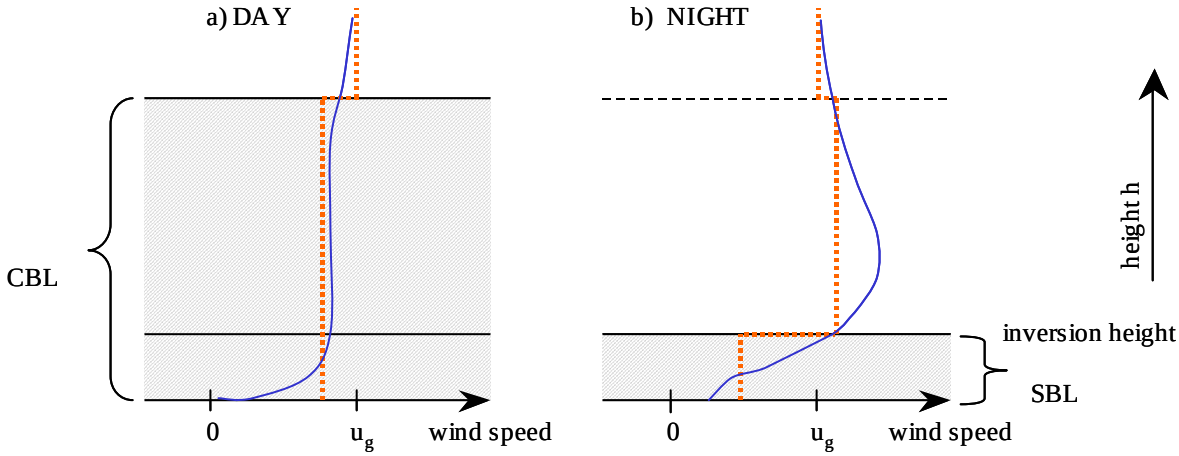

FIGURE A1: Illustration of the daytime and the night time situation in the slab model to explain the development of a nocturnal low level jet. Shaded regions mark the layers in which the stress, τ, is nonzero. The dotted line is the model assumption, the dark line is the 'realistic' case of the wind speed (adapted from THORPE & GUYMER 1977).

This model is the basis for the following explications. The development is split up in four phases:

(i) Daytime (THORPE & GUYMER 1977)

During daytime the atmosphere consists of two layers: the free atmosphere and the CBL. It is assumed that wind is geostrophic in the free atmosphere and logarithmic in the CBL. Due to the turbulent mixing the momentum is evenly distributed in the whole CBL. Pressure gradient force, Coriolis force, and frictional force are in equilibrium.

(ii) Transition period (MAHRT 1981)

Nocturnal accelerations and intensity of the low level jet appear to be enhanced by an increase of the low level ageostrophic flow generated by increased stress divergence in the lower layers due to the fact that the surface stress decreases more slowly than the

downward transport of momentum associated with decreasing depth of the turbulence. An imbalance between the stress-divergence, pressure gradient force and Coriolis force is created as the stress divergence increases, causing an acceleration across the inversion. In modelling studies, the transition period is normally omitted or replaced with an instantaneous collapse (e.g. THORPE & GUYMER 1977).

(iii) Night time

Over flat terrain DAVIES (2000) specifies two processes for the formation of a nocturnal low level jet: the inertial oscillation (BLACKADAR 1957, THORPE & GUYMER 1977) and the 'quasi-steady' state of the SBL (NIEUWSTADT 1984). At sunset it is assumed that the CBL breaks down, the two layers of the PBL become decoupled, and the upper layer of the PBL is instantly released of all frictional constraints. Assuming for simplicity furthermore that the horizontal pressure gradient is constant with time and in each horizontal plane the equations of motion for this upper layer may be written

$$\frac{du}{dt} = + f v \tag{A.1}$$

$$\frac{dv}{dt} = - f u \tag{A.2}$$

where u and v are the horizontal wind components, t is the time, and f is the Coriolis parameter. The solution of this two equations is a second order equation, thus an oscillation. In other words, the remaining gradient force and the Coriolis force try to reach a new equilibrium. As the inertial oscillation is a slow motion with a rotation period of about twelve hours for the EBEX2000 site, this new equilibrium can not be attained until sunrise. NIEUWSTADT (1984) showed that the stable layer associated with the nocturnal inversion reaches a steady state, i.e. turbulent fluxes are not a function of time. This denotes that the time scale of turbulence is usually much smaller than the time scale of the mean variables. Consequently, turbulence is continuously in equilibrium with the slowly changing mean field.

(iv) Sunrise

At sunrise convective mixing starts again, the inversion becomes destroyed and also the low level jet disappears just 2-3 hours after sunrise.

FIGURE A2 shows some examples for the appearance of the low level jet during EBEX2000. After sunset wind speed rises significantly with directions from NW. The area of the highest values is situated at a height of 150 m – 300 m and maximum values are measured shortly after midnight. The layer with strong winds decreases both in terms of thickness and speed towards sunrise. Due to the beginning convection after sunrise the low level jet decreases even stronger and has entirely vanished about three hours later.

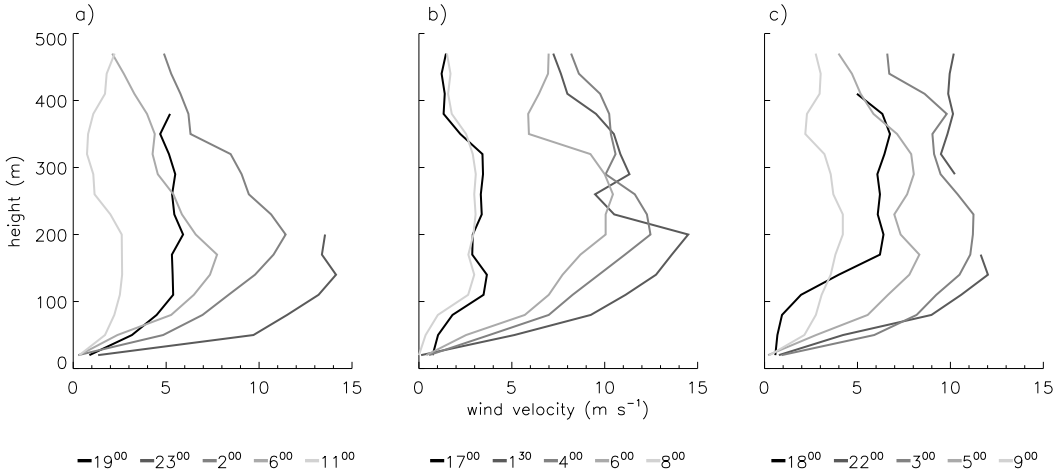

FIGURE A2: Wind profiles: a) 07./08.08.2000, b) 09./10.08.2000 und c) 10./11.08.2000 (local time).

Appendix B: Radiation sensor comparison

Each component of the radiation balance was measured by at least two different kind of sensors (see section 3.3). The decision which composite of sensors is used is based on the following comparison (Figure B1).

Incoming short-wave radiation

The values of both CM21 sensors do agree within 1 %, i.e. the difference is maximal 10 W m^{-2}. In the early morning the CM21#004 measures a few Watt per meter square more than the CM21#239, but throughout the remainder of the day about 5 W m^{-2} less. The difference shows a diurnal behaviour with one maximum around 2 pm and a second one at 7 pm. The CNR1 shows a diurnal behaviour with generally a few percent lower values than the CM21#239, with a maximum of about -20 W m^{-2} in the afternoon.

Outgoing short-wave radiation

The data of CNR1 are generally lower than the CM11 values (except around sunrise and sunset), about -15 W m^{-2} (15 %) in the morning and afternoon, and about -10 W m^{-2} (5 %) around midday.

Incoming long-wave radiation

The comparison between the CNR1 and PIR#323 shows a pronounced daily pattern with larger values for the CNR1. At night, the difference is about 5 W m^{-2} (1 %), and at midday about 25 W m^{-2} (7 %).

Outgoing long-wave radiation

The comparison of the two sensors (PIR#207 and CNR1) shows a diurnal behaviour, but within a range of ± 1%. During daytime the CNR1 shows larger values (about 5 W m^{-2}). The daily course of the difference of the long-wave incoming and outgoing radiation and its correlation with short-wave radiation is probably an indication that the CNR1 filter transmits not only long-wave radiation but also a part of the short-wave radiation.

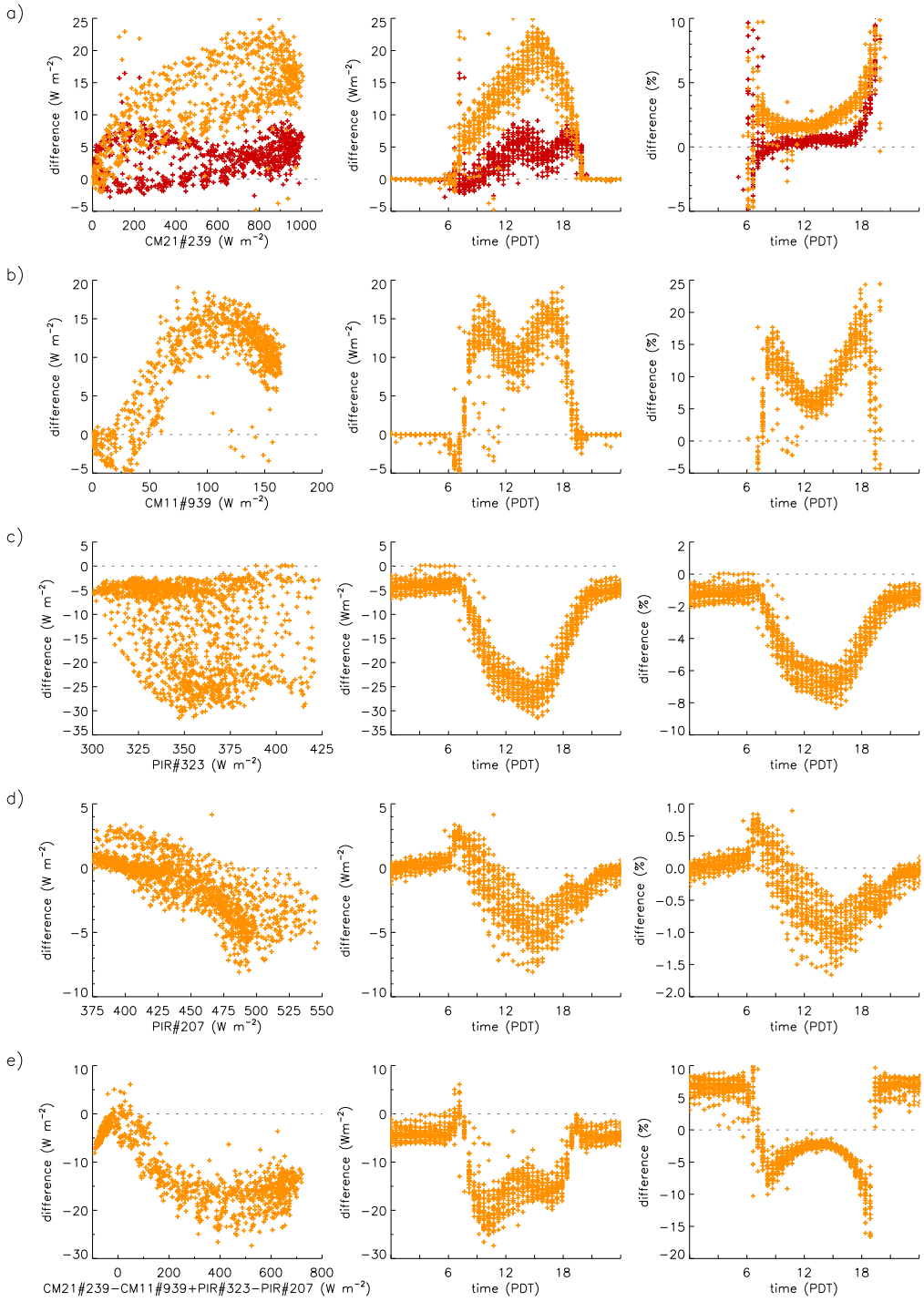

FIGURE B1: Difference in the measurement of each part of the radiation balance with different sensors (absolute value and percentage):

a) incoming short-wave radiation: black: CM21#239 – CM21#004,
grey: CM21#239 – CNR1#098,
b) outgoing short-wave radiation: CM11#939 – CNR1#098,
c) incoming long-wave radiation: PIR#323 – CNR1#098,
d) outgoing long-wave radiation: PIR#207 – CNR1#098, and
e) radiation balance: (CM21#239-CM11#939+PIR#323-PIR#207)- (CNR1#098).

Radiation balance

The radiation balance is calculated on the one hand with the four sensors of the CNR1 and on the other hand with the sensor combination CM21#239, CM11 and the two PIR's. The difference between them is mainly given by the difference in incoming long-wave radiation. Net short-wave radiation of the CNR1 is about 5 W m^{-2} smaller, but net long-wave radiation is about 20 W m^{-2} higher. The CNR1 balance shows higher values throughout the day: at night about 5 W m^{-2} and during daytime about 15 W m^{-2}.

Conclusion

The leak in the filter of the long-wave radiation sensor of the CNR1 leads to an overestimation of the long-wave radiation. The CM21#239, PIR#323, and PIR#207 were calibrated at the WRC. That means for the pyanometer, that the direct solar radiation is obtained from the World Standard Group and the diffuse radiation is determined from a shaded standard pyranometer. For the long-wave instruments no standardised calibration procedures exist. However, the pyrgeometers are calibrated with a black-body radiation source and include the determination of the needed factors to be able to carry out the correction according to PHILIPONA ET AL. (1995). Thus, the data of the sensor combination seems to be more reliable and was used as reference for the radiation.

Appendix C: Soil sensor comparison

Heat flux plates

Figure C1 shows the diurnal course of the uncorrected soil heat flux measured by heat flux plates for the time period DOY 207 – 234. There are large differences between the measurements at the ridge and in the furrow. After each irrigation (indicated by an arrow) the courses get closer. Thus, it is suggested that the two heat flux plates in the furrow were still in contact with air until DOY 230. An other reason for this estimation is the fact that the values are very high. Often the soil heat flux is parameterised as a part of the net radiation. For example 10 % by daytime (STULL 1988). As can be seen in section 3.2 the maximum value of the mean net radiation is about 700 W m^{-2}. Thus, the values of the "furrow-sensors" with more than 100 W m^{-2} are definitely too high. On the other hand the "ridge-sensors" seem to be too low. Anyhow, their values are more reasonable and their mean is used in further calculations.

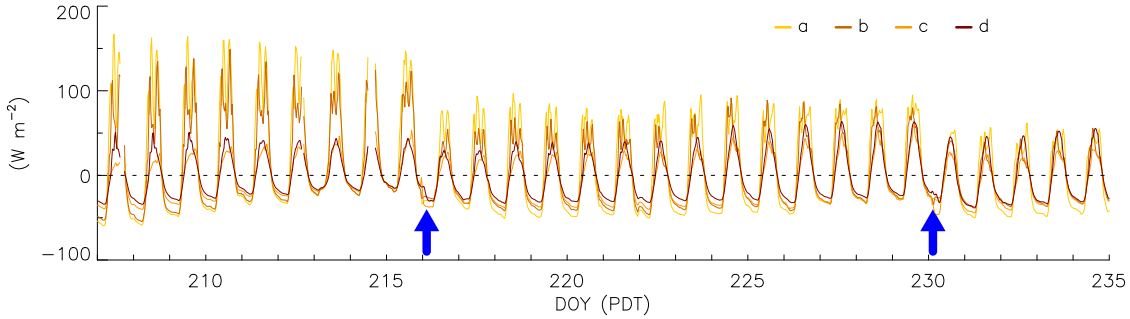

FIGURE C1: Heat flux plates fluxes (W m^{-2}) measured in a depth of 3 cm. a: furrow, b: furrow, c: south-slope of a ridge, and d: north-slope of a ridge. The arrows indicate the arriving water front.

Soil temperature sensors

As described in section 3.4.2 the value of the heat flux plates have to be adjusted for the part of the soil above the sensor. For this correction the soil temperature in a given depth is needed. Figure C2 illustrates the course of the four soil temperature sensors for the same time period as shown in figure C1. The data series show the same behaviour as the heat flux plates described above, i.e. they were not charged with water and therefore still in contact with air until DOY 230. Thus, for the correction the mean value of the two "ridge-sensors" is used.

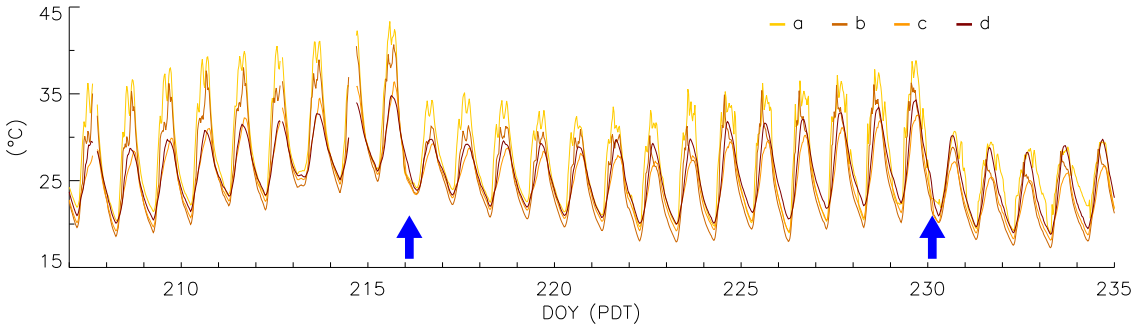

FIGURE C2: Soil temperature (°C) measured in a depth of 3 cm. a: furrow, b: furrow, c: south-slope of a ridge, and d: north-slope of a ridge. The arrows indicate the arriving water front.

Appendix D: Sonic data handling - method comparison

There are mainly three methods concerning the rotation of the coordinate system of sonic data: double rotation ($\bar{v}=0$ and $\bar{w}=0$, according to KAIMAL & FINNIGAN 1994), triple rotation ($\overline{w'v'}=0$), and planar fit ($\bar{v}=0$ and normally $\bar{w}\neq 0$, according to WILCZAK ET AL. 2001, see section 3.5.1). Triple rotation is not considered for the present study. Two other issues are the necessity of a linear detrending and the alignment of the coordinate system into the mean wind. The main difference between double rotation and planar fit is the regarded time period to calculate the rotation angles. For double rotation these angles are calculated for each single run while for the planar fit method they are always the same (as long as the tilt of the sonic is constant). To get an idea of the influence of the different methods on kinematic temperature flux $\overline{w'\theta'}$ and kinematic moisture flux $\overline{w'q'}$ and therefore their influence on the energy balance, a comparison was done with the sonic data of position A2. Figure D1 shows this comparison including the result of a linear regression. There are differences between the individual methods, but they are mostly within a few percent and thus for the present problem of energy balance closure negligible. For further calculations the planar fit method is applied due to the fact that the calculation of the rotation angles is less susceptible to sampling errors than double rotation because many data runs are used.

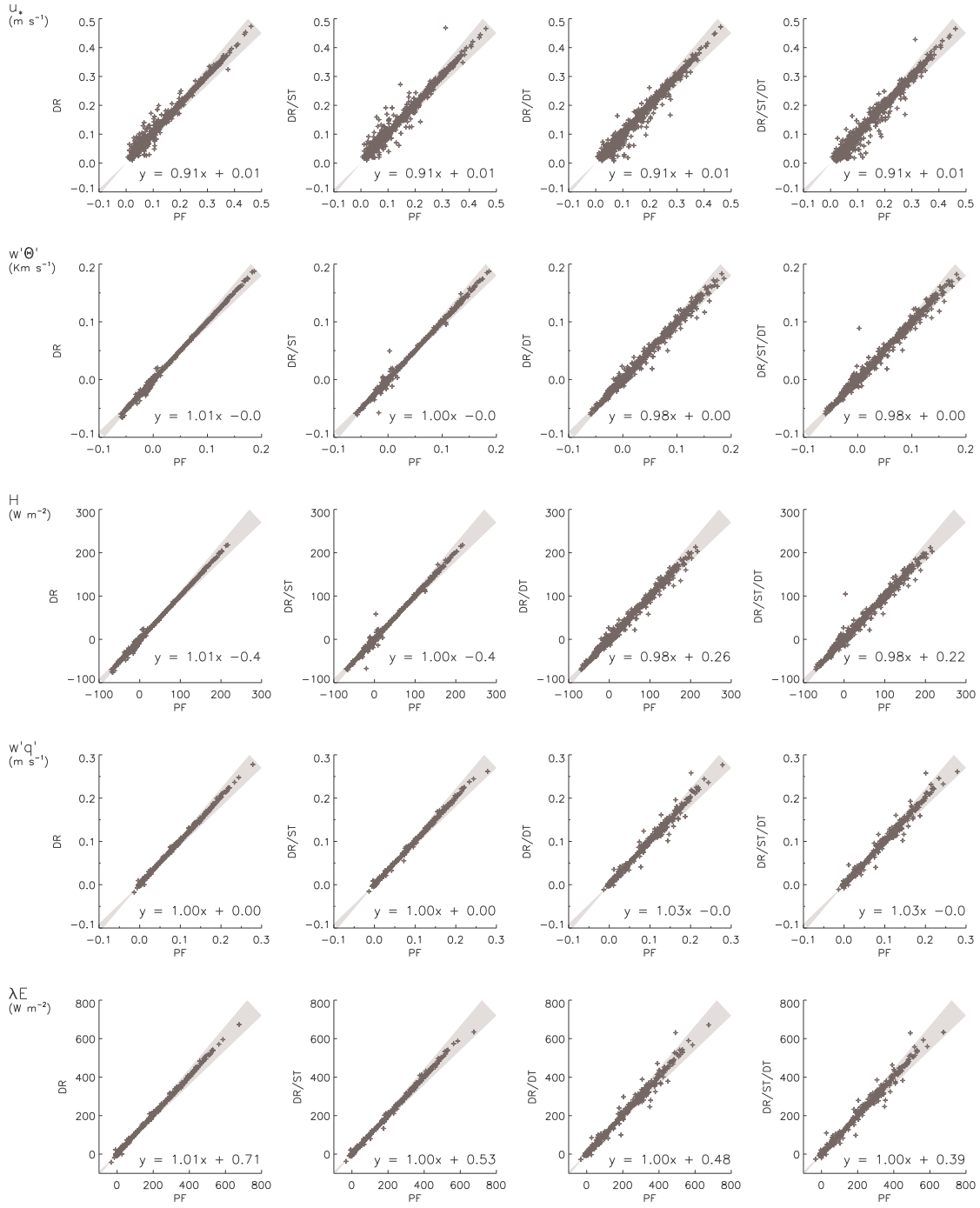

FIGURE D1: Comparison of double rotation (DR) vs. planar fit (PF) at position A2. From left to right: only double rotation, including streamline (ST), including linear detrending (DT), and including both streamline and linear detrending. Top down for friction velocity, kinematic temperature flux, sensible heat flux, kinematic moisture flux, and latent heat flux. Inside the grey area the differences are less than ±10 %.